

THESIS

LOGJAM ATTENUATION OF ANNUAL SEDIMENT WAVES IN EOLIAN-FLUVIAL  
ENVIRONMENTS, NORTH PARK, COLORADO

Submitted by

Julia Grabowski

Department of Geosciences

In partial fulfillment of the requirements

For the Degree of Master of Science

Colorado State University

Fort Collins, Colorado

Summer 2020

Master's Committee:

Advisor: Ellen Wohl

Daniel McGrath  
Ryan Morrison

Copyright by Julia Diane Grabowski 2020  
All Rights Reserved

## ABSTRACT

### LOGJAM ATTENUATION OF ANNUAL SEDIMENT WAVES IN EOLIAN-FLUVIAL ENVIRONMENTS, NORTH PARK, COLORADO

Sediment waves, a term that describes the fluvial transport of a discrete sediment influx, have long been studied in regard to channel response to infrequent, catastrophic events, such as mass movements or dam removal. However, few researchers have studied (1) the potential presence of sediment waves of annual or sub-annual scale in mixed eolian-fluvial geomorphic environments or (2) the role of large wood in sediment wave dispersal. This study addresses both topics through observations of North Sand Creek and East Sand Creek, which flow alongside the active sand dunes of North Sand Hills and East Sand Hills, respectively, in North Park, Colorado. The creeks experience similar seasonal, asynchronous cycles of eolian influx and fluvial transport, although North Sand Creek likely receives a greater volume of eolian sand due to intensive Off-Highway Vehicle (OHV) recreation on the North Sand Hills dunefield. Linear spectral unmixing of Landsat imagery from 1984-2019 is used to determine whether OHV recreation has resulted in vegetation loss, typically associated with elevated eolian flux, on North Sand Hills. Repeat photography and repeat measurement of terrace-like structures are used to determine whether each creek experiences a sediment wave, and repeat measurement of logjam sand wedge volume is used to examine changes in sand storage associated with logjams over time. Results indicate that North Sand Hills has lost vegetative cover in areas not fenced-off to OHV users at a rate of  $\sim 800 \text{ m}^2/\text{year}$ , and that North Sand Creek experiences a highly translative sediment wave that is attenuated by logjams. East Sand Hills, on the other hand, has gained vegetative cover throughout the dunefield,

and East Sand Creek does not experience a sediment wave. The sediment wave at North Sand Creek translates rapidly through the area of channel outside of the logjam backwater and translates more slowly through logjam backwater areas—principally through reduction in the length of logjam sand wedges, rather than reduction in depth.

## ACKNOWLEDGEMENTS

Thanks to Ellen Wohl and the rest of the fluvial lab for inspiring me daily with their excellent work and dedication to rivers.

Thanks to Dan McGrath and Ryan Morrison for teaching me about remote sensing and river restoration, and for supporting this project along the way.

Thanks to my field assistant Spencer Rhea for never forgetting the rebar.

Thanks to everyone at State Line Ranch for making this project possible and giving me a place to stay in the field last summer. Extra thanks to Bob for letting us borrow the Jeep and rescuing me and Spencer on several occasions.

Thanks to Paula Belcher and John Monkouski at the BLM Kremmling office and Jerod Smith with the Colorado State Land Board for helping me learn more about the history of the sand hills and helping me access them for my research.

Finally, thanks to my cat and quarantine companion, Moby.

## TABLE OF CONTENTS

ABSTRACT.....	ii
ACKNOWLEDGEMENTS.....	iv
1. Introduction.....	1
1.1 Background.....	1
1.2 Study Area.....	6
1.3 Preliminary Observations.....	9
1.4 Conceptual Model and Objectives.....	10
2. Methods.....	15
2.1 Remote Sensing.....	15
2.2 Repeat Photography.....	18
2.3 SAS Measurements.....	19
2.4 Logjam Sand Wedge Measurements.....	21
3. Results.....	27
3.1 Remote Sensing.....	27
3.2 General Field Observations.....	30
3.3 Repeat Photography.....	32
3.4 SAS Measurements.....	36
3.5 Logjam Sand Wedge Measurements.....	38
4. Discussion.....	48
4.1 Land Cover Trends Over time.....	48
4.2 Comparison of SAS and Logjam Sand Wedge Measurements.....	49
4.3 Sediment Transport Model.....	51
4.4 Management Implications.....	53
4.5 Conclusions and Suggestions for Further Study.....	55
References.....	58
Appendix A: Repeat Photography.....	63
Appendix B: Logjam Sand Wedge Measurements.....	69

## **1. Introduction**

This study addresses two poorly understood aspects of sediment waves: how they operate on annual cycles in mixed eolian-fluvial environments, and how in-channel large wood contributes to sediment wave dispersal. These questions are approached through observations of two rivers in North Park, Colorado—both of which are adjacent to active sand dunes; experience seasonal, non-synchronous fluxes in sediment load and discharge; and include relatively high densities of channel-spanning logjams. The conceptual model and objectives of this study are presented in section 1.4.

### *1.1 Background*

G.K. Gilbert first used the term sediment wave to describe the fluvial transport of hydraulic mining debris from headwater areas in the Sierra Nevada to the San Francisco bay (Gilbert, 1917). Sediment waves—also called “slugs” and “pulses”—describe the downstream movement of a spatially and temporally discrete sediment influx to a channel. According to the classic Gilbert model, the wave moves through both translation and dispersal, and is evident by at-station aggradation and channel widening, followed by incision, channel narrowing, and the formation of terraces. Sediment waves have been well-documented to be associated with infrequent, catastrophic events, such as: dumping of mining debris (Gilbert, 1917; Pickup et al., 1983; Knighton, 1989), mass movements (Nakamura, 1966; Miller & Benda, 2000; Sutherland et al., 2002; Brummer & Montgomery, 2006; Hoffman & Gabet, 2007; Pierson et al., 2011; Short et al., 2015; Nelson & Dubé, 2016), anthropogenic deforestation (Roberts & Church, 1986; Madej & Ozaki, 1995; Pryor et al., 2011), and dam removal (East et al., 2015; Pace et al., 2017). Sediment waves have also been studied in flumes and with numerical modelling (Lisle et al., 1997; Cui et al., 2003; Ferrer-Boix et al., 2014; Gran & Czuba, 2017).

A great deal of the research on sediment waves has focused on determining the relative importance of translation and dispersal in propagation. Sediment waves composed of gravel-sized and coarser material (e.g. Pace et al., 2017), which tend to disperse with little or no translation, are well-represented in literature. Studies of sediment waves composed of sand-sized sediment are rare, though the few case studies of sediment waves of predominantly sand material (Meade, 1985; Knighton, 1989) document rapid translation.

The term “sediment wave” has typically been reserved to describe fluvial transport following infrequent, catastrophic sediment influxes; however, I propose the term should also be used to describe events of annual or sub-annual timescales in rivers where seasonal fluctuations in sediment supply and discharge are asynchronous. These may include some rivers dominated by snowmelt (Paige & Hickin, 2000; Meade, 1985), and those subject to seasonal eolian influx. These rivers may experience cycles of aggradation and incision that are analogous to the sediment waves described in the studies cited above.

In-channel large wood plays an important role in trapping and storing sediment in most rivers in forested ecosystems (e.g. Wohl & Scott, 2016). Large wood therefore likely plays an important role in the dispersal of sediment waves, especially as some of the events that introduce large amounts of sediment to a channel—such as debris flows—also introduce large amounts of wood. A few researchers have made tangential observations about the relationship between large wood and sediment waves, but with one exception (Short et al., 2015), no one has studied it directly. Short et al. (2015) found that the formation of logjams and beaver dams in a mountain stream following a stand-replacing wildfire resulted in a near-halt of a sediment wave initiated by associated debris flows. Additionally, Miller and Benda (2000) observed a logjam continuing to store a kilometer-long sediment wedge for years following the downstream translation of a



sediment wave in the rest of the channel. The dearth of discussion of large wood in sediment wave literature may be due to a combination of wood being overlooked by researchers as well as the continuing legacy of human removal of wood from rivers.

While both of the creeks included in this study are adjacent to active sand dunes and are subject to eolian influx, influx into North Sand Creek is likely higher due to the management of the North Sand Hills dunefield by the US Bureau of Land Management (BLM) as an Off-Highway Vehicle (OHV) recreation area. Visitors are allowed to ride OHVs on the active sand dunes, on established paths within adjacent vegetated eolian deposits, and within North Sand Creek channel itself. OHVs, which include ATVs, UTVs, dirt bikes, and dune buggies, have a variety of negative impacts on landscapes, including soil compaction, erosion, vegetation disturbance, noise pollution, dust pollution, and animal habitat fragmentation (Ouren et al., 2007). Previous studies have clearly illustrated the tremendous erosive power of OHVs, with results including 10-20 times greater sediment yield on hillslopes that had experienced intensive OHV use than on control hillslopes in the Mojave Desert (Iverson et al., 1981); 10-25 times greater sediment deposition in sediment traps in arid watersheds in California State Vehicular Recreation Areas than in control watersheds (Tuttle & Griggs, 1987); and over 20 times higher average eolian sediment flux in OHV recreation areas on the Colorado Plateau than in areas with intensive grazing, unpaved roads, or control areas (Nauman et al., 2018). In-channel OHV recreation also impacts fluvial systems directly. A study of OHV stream crossing points in the Ouachita National Forest found 30-45 cm of erosion on adjacent banks, and evidence for downstream aggradation at 93% of sites examined (Marion et al., 2014). The BLM has acknowledged resource damage from OHVs at North Sand Hills and has fenced off some parts of the dunefield as “restoration areas,” beginning in 1988 (SEH, 2007).

In this study, linear unmixing of aerial imagery is used to quantify the impact of OHV recreation on vegetation on the North Sand Hills dunefield. Most dunes in both North Sand Hills and East Sand Hills are parabolic-type, which depend on sparse vegetation for their structure, resulting in instability and elevated eolian transport rates when the vegetation is disturbed (Ahlbrandt & Andrews, 1978). Therefore, vegetation loss is likely associated with elevated eolian transport on the dunefields, and ultimately aggradation in North Sand Creek. OHV users on North Sand Hills are only allowed to ride in areas of “open sand” on the dunefield. Some vegetated areas are physically fenced off to riders, although other areas are not, and enforcement is limited (SHE, 2007). Fencing off vegetated areas likely reduces impact, although the effect of elevated eolian transport from adjacent unfenced areas on recovering vegetation is unknown.

I apply linear spectral unmixing (Keshava, 2003) to Landsat imagery covering a period from 1984-2019 in order to estimate the rate of vegetative cover over time on both dunefields and in vegetated areas in particular. Spectral unmixing is a classification method for estimation of subpixel abundance of endmember classes (e.g., sand and vegetation) based on the linear distance of each pixel’s measured spectral profile to defined spectral profiles of endmember classes. The method is best for analysis of study areas with 2 or 3 endmember classes with easily distinguished spectral profiles, when using imagery datasets of medium or coarse spatial resolution. Meter- to sub-meter scale imagery with national coverage was not available for purchase until IKONOS-2 was launched in 2000, and not freely available until the National Agriculture Imagery Program (NAIP) began in 2007. Time series analyses including earlier periods typically use aerial photographs, which in some cases are available starting in the 1940s, although the imagery is temporally sporadic, of varying spatial and spectral resolution, and often distorted. Researchers may also use datasets such as Landsat 4 and 5, freely available from 1982-2013 with 30 m spatial

resolution, or purchase SPOT 1-3 imagery, available from 1986-2009 with 10-20 m spatial resolution (Belward & Skøien, 2015). Many features on Earth's surface occupy much smaller spatial footprints than 10-30 m, resulting in abundant mixed pixels, which at small scales reduce the efficacy of simple endmember classification.

In linear spectral unmixing, endmember spectra are defined by either supervised or unsupervised methods, and each pixel is modeled as a fractional sum of several spectral profiles (Keshava, 2003). Spectral unmixing can be described as a method to effectively improve the spatial resolution of imagery, in that more information can be gathered from each pixel, although it cannot resolve the subpixel spatial distribution of endmembers. This method has proven effective for ~35-year time series analyses with Landsat imagery, including snow and ice extent in the Andes (Cortés et al., 2014), desertification in China (Sun, 2015), and mangrove abundance on the Australian coast (Lymburner et al., 2020).

While the problem of OHV-induced erosion on dunefields and associated aggradation in rivers may seem niche and irrelevant to wider-scale problems, it is worth considering that: parabolic sand dunes are highly sensitive to physical disturbance (e.g. Yan & Baas, 2018); the BLM estimated that its lands saw 7.771 million visitor-days of OHV recreation in 2017 (BLM, 2018); 20 continental dunefields in the western US are under BLM management and are open to OHV use, including the Algodones Dunes, CA, Sand Mountain, NV, Christmas Valley Sand Dunes, OR, Juniper Dunes, WA, Coral Pink Sand Dunes, UT, Red Sands, NM, and the Killpecker Sand Dunes, WY; with increasing aridity from climate change (e.g. Abatzoglou & Williams, 2016), dunefields will grow even more sensitive to OHV-associated vegetation loss; and downstream users will be even more negatively affected by limited hydrologic conductivity associated with stream aggradation.

## 1.2 Study Area

An unnamed tributary of North Sand Creek and the East Sand Creek mainstem flow along the southeastern margins of the North Sand Hills and East Sand Hills dunefields, respectively (Fig. 1). For the sake of simplicity, I will generally refer to the unnamed North Sand Creek tributary as North Sand Creek. The North Sand Hills and East Sand Hills dunefields are each about 2 km<sup>2</sup> in area and are located about 10 km apart along the base of the Medicine Bow mountains in North Park, CO. The active sand dunes are mostly parabolic-type and are a small part of a 65 km<sup>2</sup> Pleistocene-age inactive dune complex derived from glaci-fluvial sediments (Ahlbrandt & Andrews, 1978). The creeks and their tributaries head at about 3000 m, flow alongside active dunes for about 1 km, and at between 2400 and 2450 m of elevation drain into the Canadian River, a tributary of the North Platte. Their watersheds transition from forests composed of lodgepole pine (*Pinus contorta*), limber pine (*Pinus flexilis*), ponderosa pine (*Pinus ponderosa*), subalpine fir (*Abies lasiocarpa*), and aspen (*Populus tremuloides*) to a sagebrush (*Artemisia tridentata*) steppe ecosystem at an elevation of approximately 2600 m. North Park has a semi-arid, subalpine climate, with average daily temperatures ranging from -5.9 to 11.4 °C, 27.8 cm average annual precipitation, and generally consistent snow cover between December and April (WRCC, 2020).

Both creeks are subject to strong seasonal control of both flow and sediment influx. Flow is dominated by snowmelt in the early summer. Flow in both creeks peaks in June and reaches its lowest point in February, with the difference between the two values estimated at over 30-fold (USGS, 2016). Sediment influx to the creeks is dominated by eolian transport and gravitational slumping from the active sand dunes. Delivery of sand is limited during the winter when the dunes are buried in snow and interstitial pore space is frozen. Although wind speed seasonally peaks in January, dune drift potential on both dunefields peaks in the late summer and fall months when

wind speeds are moderate and snow events are infrequent (Ahlbrandt & Andrews, 1978). Due to the non-synchronous seasonal patterns of high sediment influx in the autumn and high discharge in the early summer, both North Sand Creek and East Sand Creek may experience annual sediment waves.

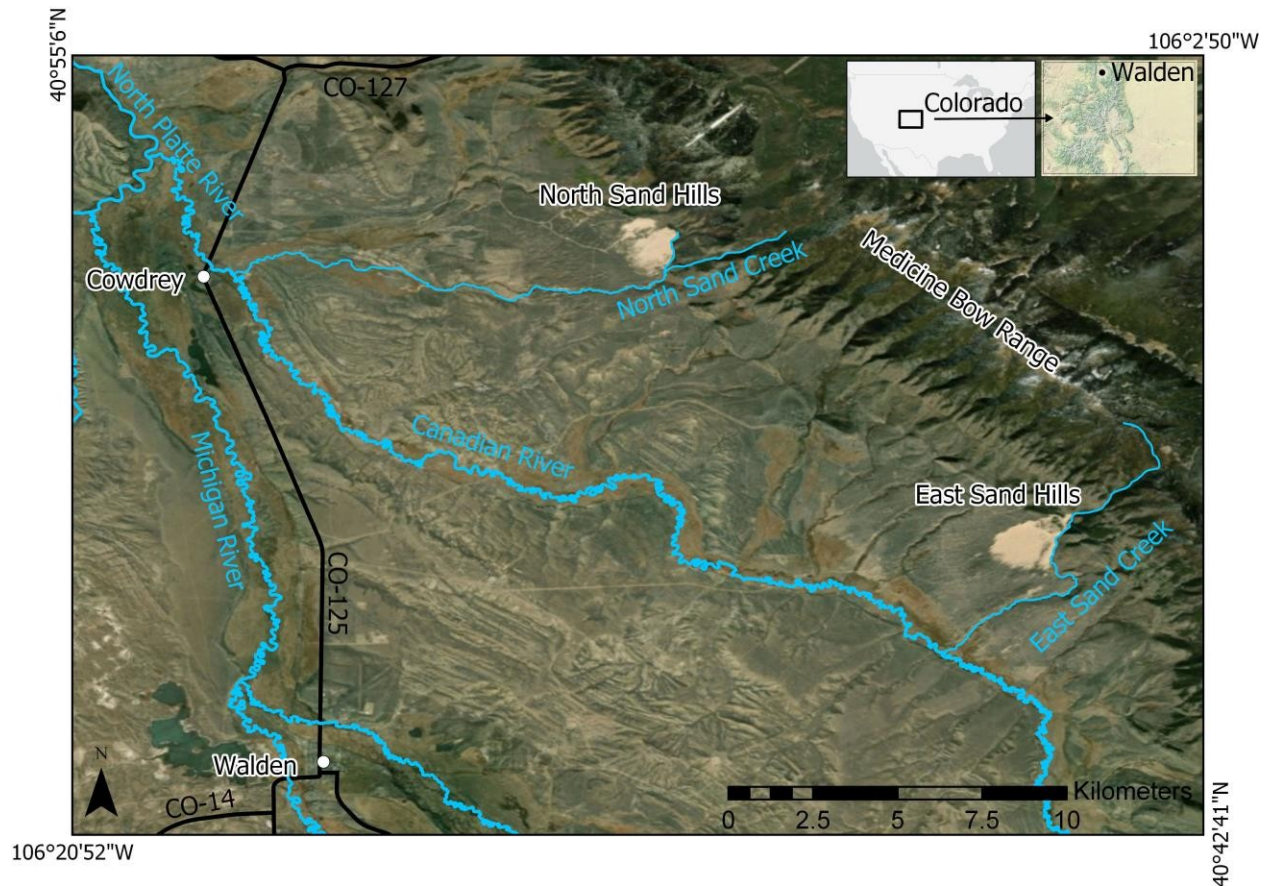


**Fig. 1.** Site map of the study area, including North Sand Hills, North Sand Creek, East Sand Hills, East Sand Creek, and the nearby towns of Walden and Cowdrey and nearby roads. The inset map in the top-right displays Colorado’s location within the continental US, and the town of Walden’s location within Colorado. Imagery source from ArcGIS Pro: ESRI, DigitalGlobe, Earthstar Geographics, CNES/Airbus DS, USDA, USGS, AeroGRID, IGN, and the GIS User Community

The two creeks, while similar in many respects, differ most notably in their drainage areas and the management of their watersheds. East Sand Creek has a drainage area of 5.9 km<sup>2</sup> just upstream of the dunefield, joins with a few minor tributaries as it flows alongside the dunes, and as it exits the dunefield area has a drainage area of 9.0 km<sup>2</sup>. The mainstem North Sand Creek, on

the other hand, does not flow directly alongside dunes. However, a tributary does, beginning with a drainage area of 1.5 km<sup>2</sup> just above the dunefield and exiting the active dune area with 2.1 km<sup>2</sup>. The tributary joins with the mainstem just downstream of the dunefield, resulting in a total drainage area of 5.4 km<sup>2</sup> (USGS, 2016). East Sand Creek therefore drains a notably larger area throughout the study areas.

East Sand Hills is managed by the Colorado State Forest Service, is not accessible to the public by road or trail, and is closed to OHV recreation. North Sand Hills, on the other hand, is managed by the BLM and has seen severe impacts from recreational visitors (SEH, 2007). In 1976, the BLM designated much of the dunefield as a Wilderness Study Area (WSA), requiring the agency to manage it in accordance with the Wilderness Act of 1964 until the US Congress either formally designated it as a Wilderness Area or released it from the WSA status, neither of which have happened to date in 2020. With what can only be called disregard to its WSA status, the BLM designated the North Sand Hills area as a Special Recreation Management Area (SRMA) for Off-Highway Vehicles (OHVs) in 1984. Yearly visitation, most of which is associated with OHV recreation, has increased over the years, with estimates of 7,500 people in 1995 and 20,000 in 2006 (Boyer, 2015). Managers have additionally noted an increase in visitation following construction of a new access road and campground in 2011 (Boyer, 2015). It is worth noting that a similar dunefield under BLM management, the Killpecker Sand Dunes in WY, allows OHV use in some areas but prohibits them in those with a WSA designation (BLM, 2020).

Erosion of the North Sand Hills dunefield has resulted in documented aggradation of North Sand Creek. State Line Ranch is located about 5.5 km downstream of the dunefield and holds senior water rights to North Sand Creek. Ranch managers observed an unprecedented influx of sand into the ranch irrigation network in 2011 (Boyer, 2015). The sand influx continues to date

and has resulted in significant loss of utility of ranch irrigation. The Colorado State Water Quality Control Commission placed North Sand Creek on its list of waters impaired due to sediment in 2016 in response to a petition from the State Line Ranch (COWQCC, 2016).

### *1.3 Preliminary observations*

The first visit to North Sand Creek took place in November 2018. One of the most salient observations of that visit was the presence of several channel-spanning logjams. Most of these were accompanied by an upstream “wedge” of stored sediment. These wedges were composed predominantly of sand, while the bed material of the rest of the creek was predominantly cobbles and gravel. This was observed to also be the case in East Sand Creek during a first visit in May of 2019. The phenomenon of logjams trapping a sediment wedge with bed material preferentially finer than in the surrounding channel has been documented in many rivers (e.g. Wohl & Scott, 2016). Following these observations, I hypothesized that if a sediment wave does occur in the creek, large wood plays a significant role in its dispersal.

I observed evidence that historical beaver activity was important in introducing wood to both creeks, and possibly remains so. Chewed stumps and inactive dams and lodges were found throughout the creeks. Many of the logjams identified in both creeks included chewed sticks and may have originated as beaver dams. Green chewed sticks were observed in the two upstream-most logjams in East Sand Creek beginning in July 2019, indicative of modern activity. Additionally, a beaver was captured in a motion-triggered photo from a game camera in North Sand Creek, although there was no evidence for modern activity in that creek’s logjams. Where partial beaver dams remain present, they store sediment upstream in the same manner as logjams.

One unusual feature of both North Sand Creek and East Sand Creek is the presence of terrace-like structures entirely composed of sand in reaches that had previously aggraded and then

incised. Formation of terraces has been a well-documented result of sediment waves, beginning with Gilbert (1917), and including several more recent studies (e.g. Roberts & Church, 1986; Miller & Benda, 2000). Because these studies concern sediment waves of an infrequent and catastrophic nature, they produce terraces that are only rarely destroyed. The terrace-like structures in North Sand Creek and East Sand Creek, on the other hand, are likely created and destroyed every year, and are therefore not fully analogous to the structures described elsewhere in the literature on sediment waves. Moreover, given that most definitions of fluvial terraces include long-term abandonment by the channel (e.g. Anderson & Anderson, 2010), the features in these two creeks probably should not be called terraces. Similar structures likely exist in other mixed eolian-fluvial environments and appear to be documented in photographs included in studies of tributaries of the Yellow River in China (Xu et al., 2006; Ta et al., 2015), although these authors did not use any particular term to describe the features. I will refer to the terrace-like structures as Sand Aggradation Structures (SASs).

#### *1.4 Conceptual Model and Objectives*

First, given the well-established connection in literature between OHV recreation and vegetation disturbance (e.g. Ouren et al., 2007), North Sand Hills has likely experienced losses in vegetative cover on the dunefield, especially within vegetated areas that are not fenced off to OHV users. Vegetation loss implies elevated eolian transport on the dunefield, and ultimately higher sand influx to the creek. There are three hypotheses associated with the remote sensing analysis of dunefield land cover trends over time:

1. The rate of change of vegetative cover over time on the North Sand Hills dunefield is negative (representing vegetation loss), and significantly more negative than that on East Sand Hills.



2. The rate of change of vegetative cover over time in areas that are not fenced off to OHV users on North Sand Hills is negative, and significantly more negative than those that have been fenced off.
3. The rate of change of vegetative cover over time in fenced-off areas on North Sand Hills is significantly less than that of vegetated areas on East Sand Hills.

The preliminary observations at North Sand Creek indicated that sand is stored in two different ways: behind logjams in wedges, where it may persist through the winter; and outside of logjam backwater areas, where it is rapidly incised in the early summer during peak streamflow, leaving behind SASs. This study contrasts sand dynamics within these two storage areas to determine whether each creek experiences a sediment wave, and if so, whether and how logjams contribute to wave dispersal. The objectives are addressed using three types of field data: repeat photography, SAS measurement, and logjam sand wedge repeat measurement. For the purpose of simply characterizing longitudinal patterns, each creek is divided into upstream and downstream zones for analysis. The upstream zone is defined as the section of the creek directly adjacent to active sand dunes. The downstream zone is defined as the section within 1 km of the lower limit of the upstream zone. The results from each type of measurement are contrasted by creek and by zone.

Although they overlap to some degree, repeat photography and SAS measurements are generally used to examine sand storage in the creek outside of logjam backwater areas, in contrast to the sand stored in wedges behind logjams. Repeat photos are used to describe longitudinal and temporal patterns of aggradation and incision throughout both creeks. SAS measurements are used to determine an Incised Sand Volume (ISV), which quantifies the volume of sand that had previously aggraded in the channel and was subsequently removed through erosion. SASs were

measured in June and August 2019, allowing for an understanding of seasonality of aggradation and incision. I also took repeat measurements of logjam sand wedge depth and length throughout the summer of 2019, allowing for an estimation of sand wedge volume. Trends in logjam sand wedge volume are examined both by individual logjam and by the total sand wedge volume in each zone. The results of each of these analyses are used to match sediment transport dynamics in each creek to one of six possible models, as summarized in Figure 2 and Table 1.

Previous research has established rapid translation of sediment waves composed of sand-sized material (Meade, 1985; Knighton, 1989); long-term storage of sediment wave material behind logjams (Miller & Benda, 2000; Short et al., 2015); and the critical role of large wood in in-channel sediment storage in general (Wohl & Scott, 2016). Based on this research, I have two hypotheses concerning sediment wave dynamics in North Sand Creek and East Sand Creek:

1. Both creeks exhibit an annual sediment wave that translates rapidly through areas outside of logjam backwater storage, while logjam sand storage either remains constant or changes more slowly. Logjams in the upstream zone are likely to experience a net loss of sand, while logjams in the downstream zone may experience a decrease (transport model c) or increase (transport model d) in sand storage.
2. The annual sediment wave at North Sand Creek is of a higher magnitude than that at East Sand Creek due to higher rates of eolian influx as a result of OHV recreation in the watershed.

Initial conditions	Transport model	Final conditions: Channel outside of logjam backwater	Final conditions: Channel outside of logjam backwater	Description
upstream zone	0. no sediment wave	NC	NC	There is no sediment wave.
Channel outside of logjam backwater	a. high translation with no dispersion	—	NC	The wave translates completely out of the study area.
	b. moderate translation with no dispersion	—	+	The wave translates from the upstream to downstream zone and is stored both within and outside of logjam backwater areas.
Logjam backwater storage	c. high translation with dispersion	—	NC	The wave translates and disperses within logjam backwater areas, but otherwise translates out of the study area.
	d. moderate translation with dispersion	—	+	The wave translates and disperses from the upstream to downstream zone both within and outside of logjam backwater areas.
	e. dispersion with no translation	—	+	The wave disperses both within and outside of logjam backwater areas.

**Fig. 2.** Summary of five possible models of sediment wave movement over the course of the summer with and without logjam backwater areas, given the initial conditions. The size of yellow areas symbolizes relative volume of sand storage, and the size of the minus or plus signs symbolizes relative magnitude of change from the initial conditions.

**Table 1.** Summary of evidence from each of the three measurement types supporting each of the six possible sediment transport models

Sediment transport model	Evidence		
	Channel outside of logjam backwater		Logjam backwater
	Repeat photography	SAS measurements	Logjam measurements
0. no sediment wave	No consistent evidence for incision or aggradation in either zone	No SASs in either zone	Rate of change of total logjam sand wedge storage is not significantly different from 0 in either zone
a. high translation with no dispersion	Qualitative indicators for high-magnitude incision in the upstream zone, and no change in the downstream	High ISV in the upstream zone and no SASs in the downstream zone	Rates of change of total logjam storage volume in the two zones are both significantly less than 0 and not significantly different
b. moderate translation with no dispersion	High-magnitude incision in the upstream zone and high-magnitude aggradation in the downstream zone	High ISV in the upstream zone and no SASs in the downstream zone	Significantly less than 0 rate of change in the upstream zone and significantly greater than 0 rate in the downstream zone
c. high translation with dispersion	High-magnitude incision in the upstream zone, and no change in the downstream	High ISV in the upstream zone and no SASs in the downstream zone	The rate of change in the upstream zone is significantly less than 0 and significantly more negative than the rate in the downstream zone
d. moderate translation with dispersion	High-magnitude incision in the upstream zone, low-magnitude aggradation in the downstream zone	High ISV in the upstream zone and no SASs in the downstream zone	The rate of change in the upstream zone is significantly less than 0 and significantly more negative than the rate in the downstream zone
e. dispersion with no translation	Low-magnitude incision in the upstream zone and low-magnitude aggradation in the downstream zone	Low ISV in the upstream zone and no SASs in the downstream zone	Neither rate of change is significantly different from 0.

## **2. Methods**

### *2.1 Remote Sensing*

I used the Google Earth Engine Code Editor to select images from the Landsat 5 ETM and 8 TIRS Surface Reflectance datasets (USGS, 2020a; USGS, 2020b) from the months of June to September, and which were entirely cloud-free within polygons covering both of the dunefields. A total of 90 images fit these criteria between the years 1984-2019, with a maximum of five images per year and a median of three images per year. No images fit the criteria for the years 2000 and 2012. The images were clipped to the polygons covering both dunefields and downloaded with all bands for further processing in ArcGIS Pro.

Classification criteria were developed using the Train Maximum Likelihood Classifier tool. Because the Landsat 5 and 8 imagery datasets have different bands, criteria were developed using a Landsat 5 2011 image (ID: LT05\_034032\_20110928) and a Landsat 8 2013 image (ID: LC08\_034032\_20130816) that were then applied to all images within each dataset. The schema was based on two classes representing sand and vegetation. Training polygons representing sand were defined as the open area of the North Sand Hills dunefield. Polygons representing vegetation were defined as the sagebrush and forest areas adjacent to, but not within, the dunefields. This tool produces spectral profiles, stored as ESRI classifier definition files (.ecd), representing the mean values of each band for each class. ArcGIS Pro ModelBuilder was used to process the 90 images efficiently. The 90 images were clipped into two separate raster datasets representing each dunefield (Fig. 3). They were then classified with the Linear Unmixing Tool and the classifier definition files. This tool produces a raster with separate bands representing the modeled fractional abundance of each class in each pixel.

I clipped the classified rasters further to analyze results in vegetated areas on the dunefield, in particular (Fig. 3). Vegetated areas were delineated visually based on the farthest extent of

continuous vegetation patches in either 2019 imagery in the ArcGIS Pro basemap or 3.5 m resolution CIR aerial photographs from 1989 (USGS, 1989). The vegetated areas on North Sand Hills were further divided into those that were fenced off by BLM managers as “restoration areas” before 2019, and those that were not. These areas were visually delineated from fences that were visible in the 2019 ArcGIS Pro basemap aerial imagery.

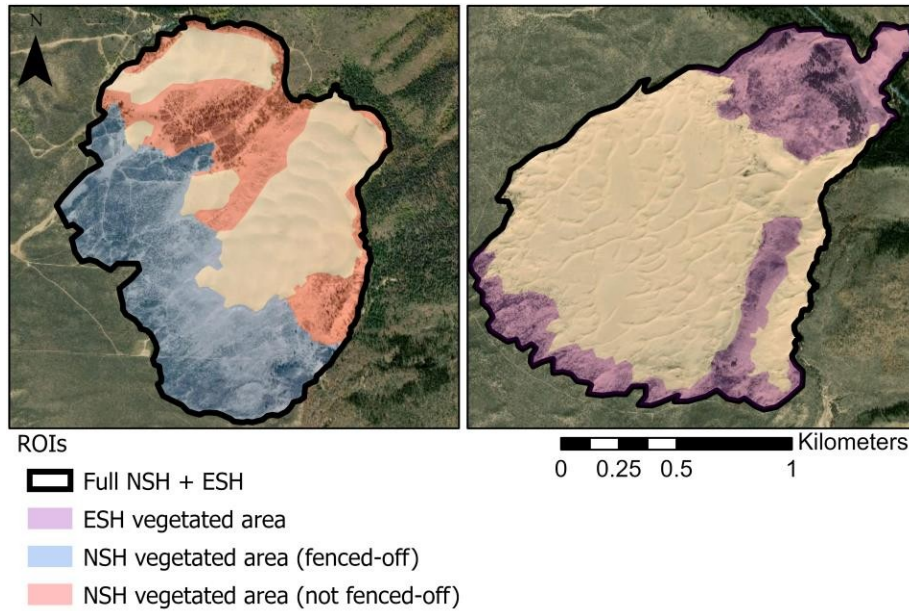


**Fig. 3.** Regions of interest used in the remote sensing analysis. The classification was performed with Landsat 5 and 8 rasters clipped to the dunefields (Full NSH + ESH), and these were later clipped for further analysis into the vegetated areas. Imagery source from ArcGIS Pro: ESRI, DigitalGlobe, Earthstar Geographics, CNES/Airbus DS, USDA, USGS, AeroGRID, IGN, and the GIS User Community

Following clipping, I further processed the classified raster data in order to sum the estimated total area of sand in both the dunefields as a whole, and in the vegetated areas in particular. I selected the raster band representing the modeled abundance of sand; transformed it into integer form; created attribute tables with the summed abundance of pixels with percentage values rounded to the tenth decimal place; created a field representing the total modeled area of sand for each pixel value; created two tables populated with the total area of sand in each image;

and finally exported these tables into Excel. Following simple processing in Excel, the data were exported into R for statistical analysis.

In R, I created two ANCOVA models in order to compare the rates of change of total estimated sand area over time between the North Sand Hills and East Sand Hills dunefields, as well as between the ESH vegetated areas, fenced-off NSH vegetated areas, and non-fenced NSH vegetated areas. The models all regressed total sand area against time (as a decimal year value), with the region of interest as a covariate. Emtrends from the emmeans package (Lenth, 2009) was used to test the significance of differences between the slopes.

One underlying assumption from these statistical comparisons is that, if the vegetation coverage on the dunefield experiences annual fluctuations throughout the summer months, the day of the year each image was collected is randomly distributed throughout the study period, such that there is no seasonal bias in the time series data. One example of the failure of this assumption might be if most of the images from the 1990's were collected during the month of June, and most during the 2010's were collected during the month of September. This assumption is checked through two statistical analyses:

- (1) A one-way ANOVA test regressing the area of vegetation against the day number value for each site, in order to determine whether the estimated area of vegetation is affected by the time of year at which the image was collected.
- (2) A one-way ANOVA test regressing the day number value against the year, in order to determine whether there is a trend in the time of year at which the imagery was collected over the study period.

## 2.2 Repeat Photography

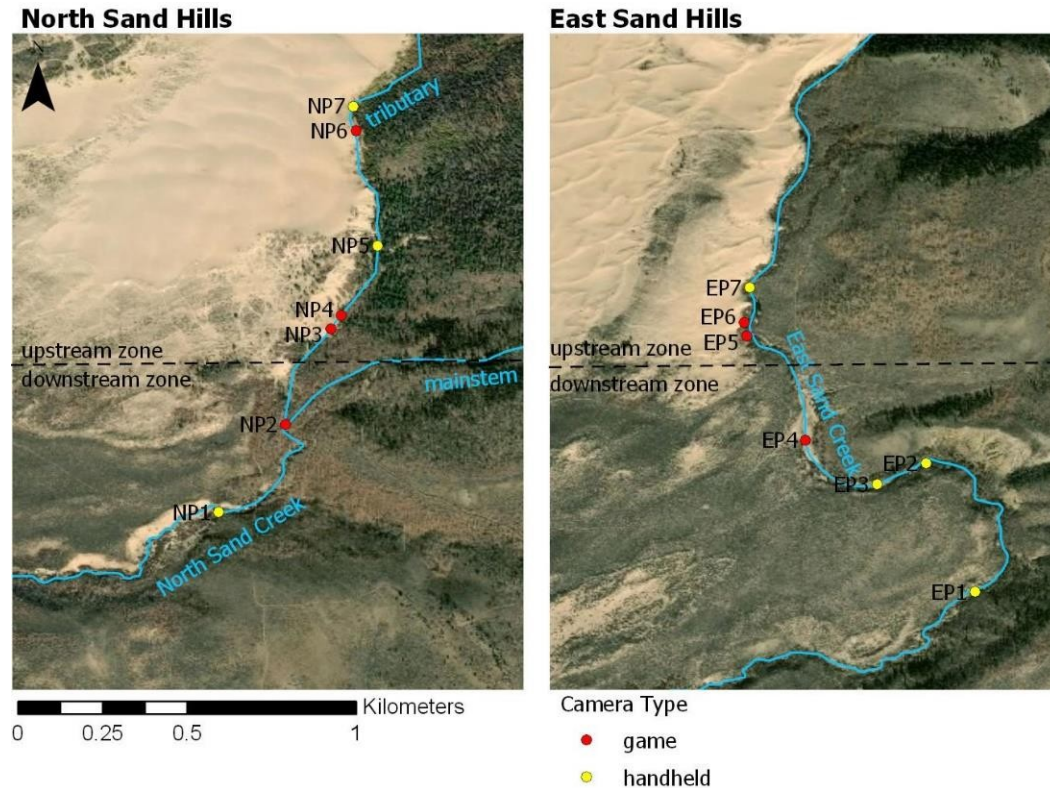


**Fig. 4.** Map of locations of repeat photos in North Sand Creek and East Sand Creek, labeled by type of camera used. Game cameras were programmed to take a photo every hour, while the handheld cameras were used during every field visit on an approximately biweekly basis.

Repeat photography was accomplished both through handheld and game cameras (models: Bushnell Trophy Cam HD Essential E2 and Bushnell Trophy Cam HD Aggressor) (Fig. 4). Game cameras were set up with the “field scan” setting in order to automatically capture one photo every hour throughout daylight hours. Four game cameras were installed at North Sand Creek during the first field visit in November of 2018. Two were installed at the creek’s largest logjam (NP16), one at the confluence of the dune-adjacent tributary with the mainstem North Sand Creek (NP2), and one at the lowermost reach of the upstream zone—a popular area for OHV users to ride in and alongside the creek (NP3). Game cameras were installed at East Sand Creek during the first field visit in the first week of June 2019. Two were installed at the lowermost logjam (E1) and one at a



dune-adjacent reach in the upstream zone (EP6). In late June, the first month of summer photos were reviewed, and the view of the channel from all four game cameras installed at logjams was obscured by in-frame vegetation. The two at North Sand Creek were subsequently moved to two other reaches in the upstream zone popular with OHV users (NP5, NP7) with better channel visibility. The two cameras at East Sand Creek were also moved to reaches in the upstream zone. One photo per day, taken at approximately the same time, were selected for each camera and finally sequenced into time-lapse videos with Adobe Photoshop.

Repeat photos were also taken with a handheld camera at flagged locations during every field visit. These locations were decided principally based on visibility of the channel without obscuration by riparian vegetation. A handheld camera was also used to take photos of every logjam coincident with the repeat sand storage measurements, which took place approximately biweekly throughout the summer.

### *2.3 SAS Measurements*

Sand Aggradation Structures (SASs) were identified and measured in each creek during the weeks of 3 June and 19 August 2019 (Fig. 5). An SAS was identified based on the following characteristics: a terrace-like morphology with a flat horizontal top; commonly, but not always, evident at the same elevation on both sides of the creek; steep, vertical sides adjacent to the channel, indicating recent incision; and an absence of grass, willow shoots, or other vegetation, indicating formation within the last growing season. The SASs at North Sand Creek commonly included several “levels,” representing the channel’s simultaneous migration and incision. Several SAS levels were observed to be about a meter vertically above logjams in the upstream zone, indicating the logjam’s previous burial. Throughout the summer, some SAS sections collapsed and some levels were destroyed.

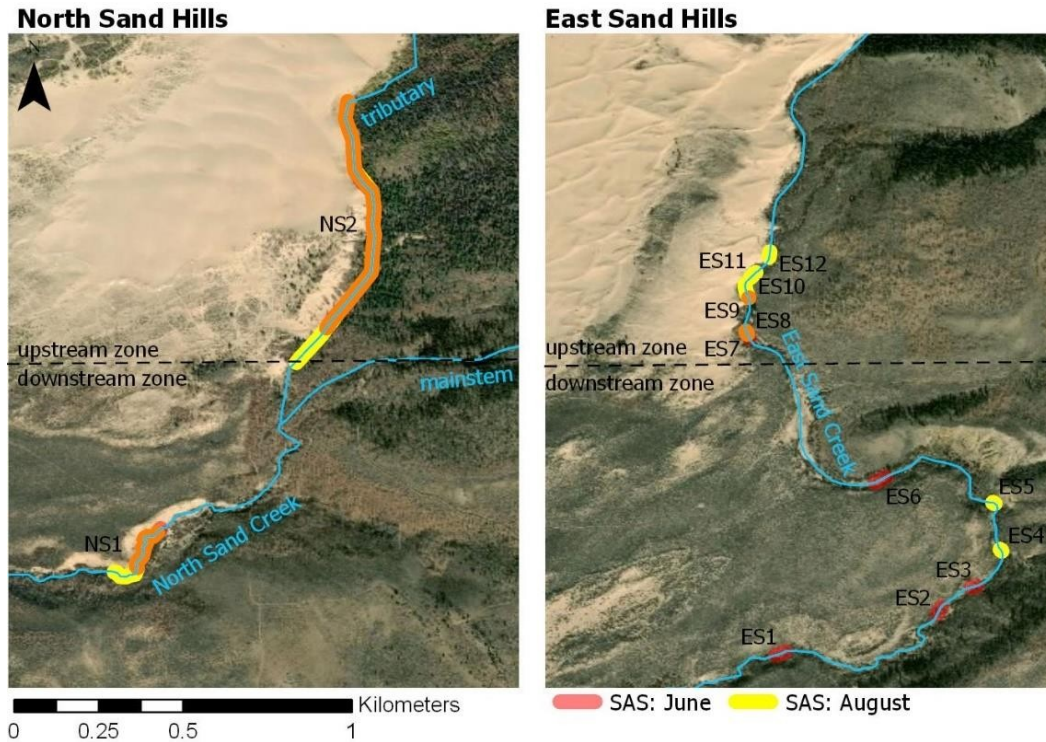


**Fig. 5.** Map of SASs identified and measured in June (red) and August (yellow) in North Sand Creek and East Sand Creek. SASs present during at both times overlap as orange.

At 10 m increments along the channel, the highest SAS on either side of the creek was identified, and a laser rangefinder was used to measure its height above the active channel to the nearest decimeter. I measured SAS width, also to the nearest decimeter, from the point at which the horizontal surface intersected the bounding slope. If the highest SAS level was extant on only one side of the channel, the full width was measured to the opposite slope at the level's approximate elevation (Fig. 6)



**Fig. 6.** Diagram illustrating the measurement of width ( $w$ ), height ( $h$ ), and the 10 m length ( $l$ ) of SAS ISV in North Sand Creek, demonstrating how ISV is modeled as a triangular prism. In this case, the highest SAS level is preserved on both sides of the channel.

Incised Sand Volume (ISV) associated with an SAS was estimated by modeling the incised sand as a triangular prism at each 10 m of the SAS length, and summing these together (Fig. 6). For 10 m increments where an extant SAS was not observed, but SAS levels were evident both upstream and downstream of the gap, it was assumed to represent a section of SAS destroyed prior to observation, and the width and height were linearly extrapolated in Excel.

#### *2.4 Logjam sand wedge measurements*

Channel-spanning logjams in both creeks in both the upstream and downstream zones were identified and marked with GPS points in late May of 2019 (Fig. 7). The logjams in both creeks were numbered sequentially starting at the downstream end. The spacing distance between the logjams was measured with a laser rangefinder for those within ~50 m of each other and using the GPS points in ArcGIS Pro for those farther apart. I calculated a “downstream distance” to define the logjam’s position in the creek by cumulatively summing the spacing distances and treating “0” as the upstream-most point in the creek adjacent to active sand dunes.

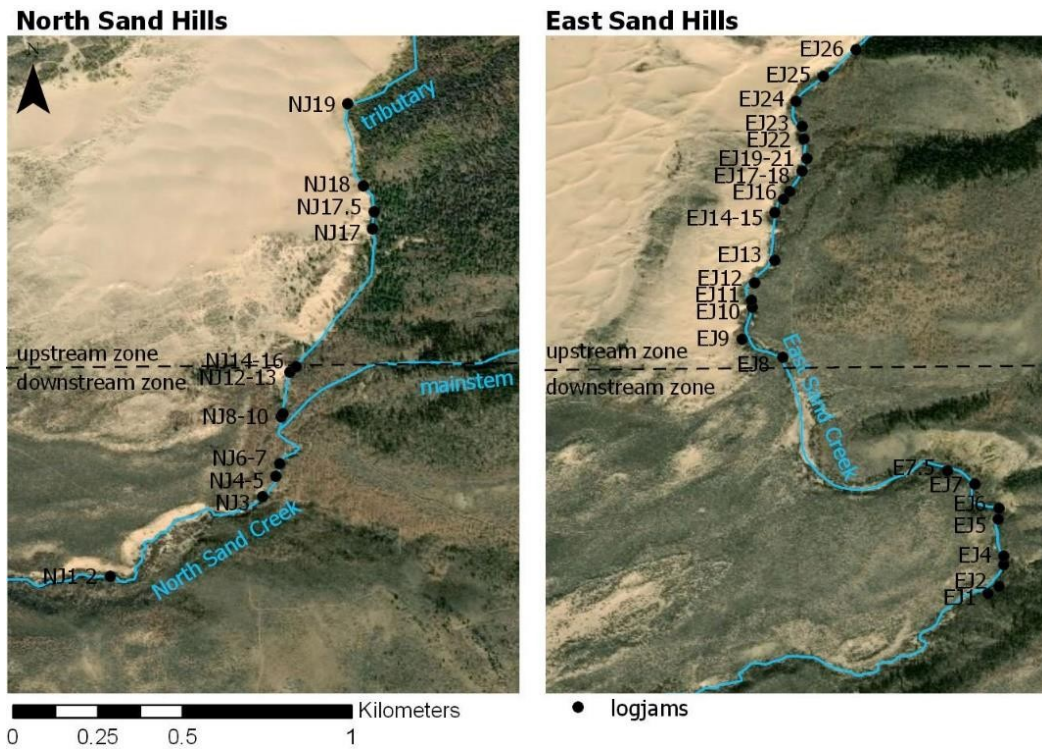


**Fig. 7.** Map of logjams subject to repeat measurements in North Sand Creek and East Sand Creek.

In each creek, two additional logjams were identified following the first week of measurements, possibly due to one or more of the following reasons: the logjams formed after the first week of observation; the logjams were uncovered from burial in sand as the channel incised; or the logjams were not initially observed because of thick riparian vegetation along the narrow channel. These logjams were numbered as “halves”—for example, logjam EJ7.5 was identified in East Sand Creek between the logjams EJ7 and EJ8 during the second week of observation.



**Fig. 8.** Diagram representing the four field measurements made at logjams that were used to calculate sand wedge volume

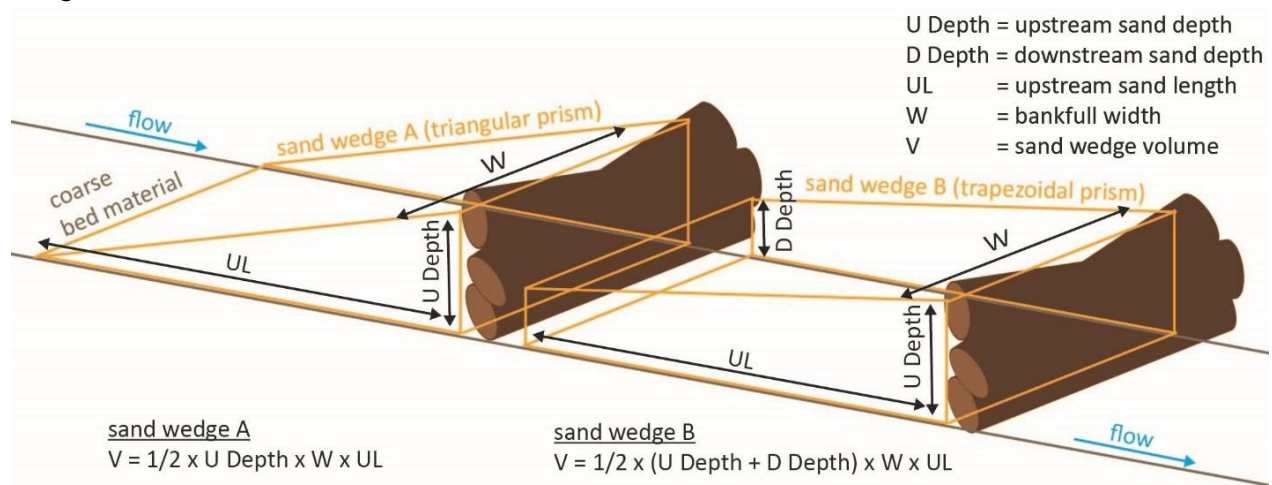


**Fig. 9.** Diagram demonstrating the calculation of sand wedge volume as either a triangular prism (sand wedge A) or a trapezoidal prism (sand wedge B)

A few of the logjams collapsed over the course of the summer and ceased to store sand. These logjams are as follows: NJ12 and EJ10 during the week of 17 June; EJ23 in 3 July; and NJ8 and NJ10 in 16 July. Additionally, BLM managers piled logs on top of the sand wedge behind NJ19 during the week of 16 July in an effort to prevent OHV riders from crossing the creek, making measurement of sand wedge volume impossible after that date.

Logjam sand wedges were measured on an approximately biweekly basis throughout the summer of 2019, during the following weeks: 21 May, 3 June, 17 June, 1 July, 15 July, 5 August, and 19 August. During all weeks, measurements at the two sites were made within one day of each other. Due to initial logistical problems with accessing East Sand Hills, measurements were not made at East Sand Creek until the week of 3 June.

Repeat sand wedge measurements involved four individual measurements: sand depth above the logjam; sand depth below the logjam; and the active channel width above the logjam (Fig. 8). Sand depth was measured within 1 m above and below the logjam. Three measurements each above and below were taken, within the left, center, and right thirds of the channel. Sand depth was measured to the nearest centimeter by driving a 124 cm-long piece of rebar into the sand with a rubber mallet, until resistance from the underlying coarse bed substrate was encountered. If the sand was deeper than the rebar, the depth was recorded as 124 cm. Only one of the logjams, NJ16, had a sand depth consistently greater than 124 cm, making the volume estimates for the NJ16 sand wedge underestimates of the true volume.

The upstream limit of the logjam's sand wedge was determined as the location in the channel where the bed substrate was approximately 75% sand and 25% cobbles and/or gravel. The distance between this location and the logjam was then measured with a laser rangefinder. If a sandbar representing less than 75% of the channel width was present, rather than a continuous sand

wedge, the sandbar length was measured and labeled as “bar.” When part of the channel was dry, as was the case for the North Sand Creek tributary in the late summer, the logjam sand wedge was measured once more, and then not again, under the assumption that fluvial transport had halted.

Logjam heights and the diameter of the three largest included wood pieces were also measured once to the nearest centimeter. Logjam height was defined as the vertical distance from the coarse bed material below the logjam—determined by driving rebar through the overlying sand layer—to the water surface above the logjam. The diameters of the logs included in the jam that appeared to be the largest were measured, and then the largest of these diameters was selected and used in analysis.

Logjam sand wedges were modelled for volume calculation as either a trapezoidal or triangular prism (Fig. 9). In both cases the bankfull width was used for the width of the prism, estimated as the active channel width during the week of 3 June. If the sand upstream length extended to the next upstream logjam, the volume was modelled as a trapezoidal prism with the upstream sand depth of that logjam and the downstream sand depth of the logjam immediately upstream as heights. Otherwise, the sand wedge was modelled as a triangular prism, using only the logjam upstream sand depth as height. If the logjam was recorded as having a sandbar rather than a continuous sand wedge, the same calculations were performed with the sandbar upstream length, and the resulting value was finally divided in half and included with the others.

Three statistical tests were used to analyze the logjam sand wedge data: (1) MANOVA test to determine whether the logjams differ among factors potentially associated with sand volume; (2) ANCOVA linear regressions of the total sand volume in each zone against time; and (3) ANCOVA linear regressions of measured variables against time at each individual logjam. R was used for all statistical analyses. The details of the three statistical analyses are below:

- (1) Four variables were measured for each logjam that I inferred to potentially be associated with sand wedge volume: downstream distance, spacing distance, height, and largest log diameter. A multivariate analysis of variance (MANOVA) test was used to test whether the mean values for all logjams differed significantly between creeks. The null hypothesis, representing not significantly different means, indicates that the capacity for sand storage behind logjams in the two creeks is similar, and we can assume that differences in sand wedge dynamics are due to differences in sand influx volume or sand transport rate, rather than due to differences in the logjams themselves.
- (2) Logjam sand storage volume values were totaled for both creeks by zone and week. These values were then regressed against time with site as a covariate, by the ANCOVA method. This model format allows for the fit of an intercept and slope for each zone; the test of all model coefficients against 0; and the test of model coefficients against each other using the emtrends function in the emmeans package (Lenth, 2009). See Table 1 for detailed descriptions of how the results of this test are used to understand sediment wave dynamics in the two creeks via the conceptual model (Fig. 1).
- (3) Three variables of the repeat logjam measurements—upstream depth, upstream length, and estimated volume—were regressed against time by the ANCOVA method with the logjam ID as a covariate. Upstream depth slopes significantly less than 0 indicate that the logjam experienced sand wedge “lowering,” upstream length slopes significantly less than 0 indicate that the logjam experienced sand wedge “shortening,” and volume slopes significantly less than 0 indicate that the sand wedge has lost sand at a significant rate. The number of logjams with significant trends in the three variables over time is compared between creeks and between



zones in order to constrain the physical dynamics of how sand is stored by and moves across logjams.

### 3. Results

#### 3.1 Remote Sensing

The linear unmixing results qualitatively agree with the density of vegetation and sand in the original rasters when displayed in natural color (Fig. 10). There are clear spatial patterns evident when classified rasters from June 2018 and June 1984 are differenced (Fig. 11). East Sand Hills has experienced a mix of gains and losses of vegetative cover within the “open sand area,” and gains of vegetation up to 75% of the pixel area within vegetated areas in particular. No pixel in the raster saw a loss of more than 25% of the vegetated area. North Sand Hills has also gained vegetative cover within the area that has been fenced off from OHVs, although some

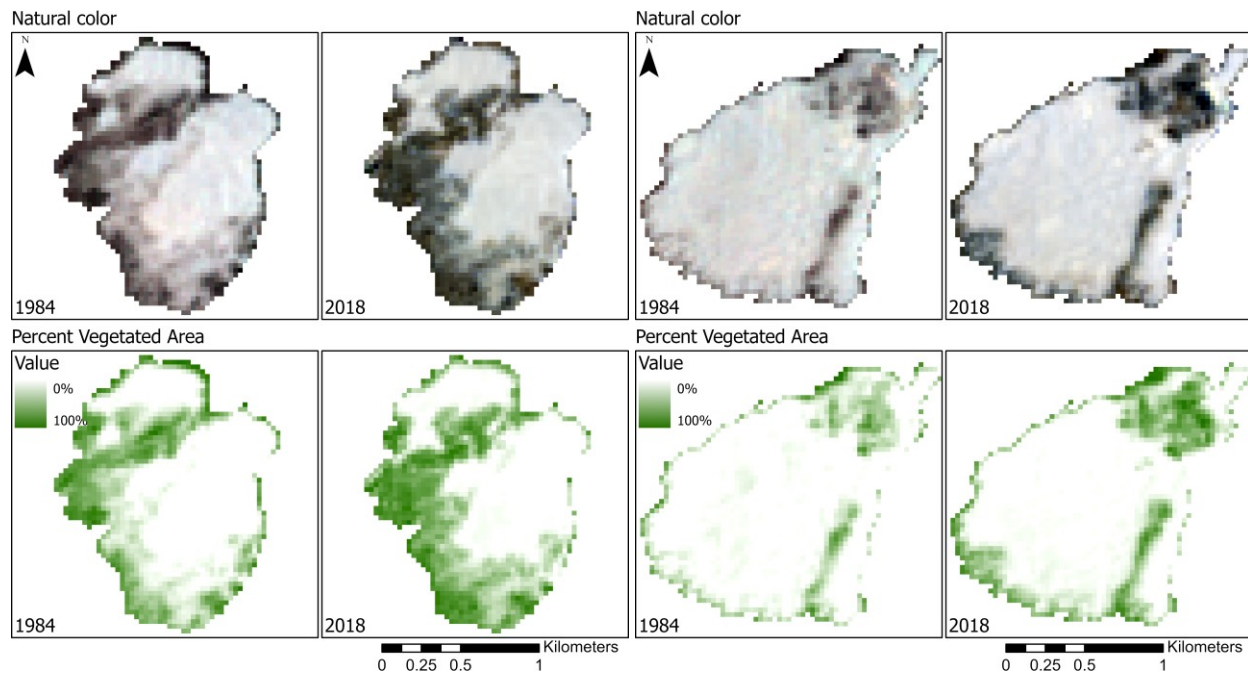


**Fig. 10.** Qualitative comparison of the Landsat rasters displayed in natural color, and the classified rasters representing percent vegetation, for North Sand Hills (left) and East Sand Hills (right).

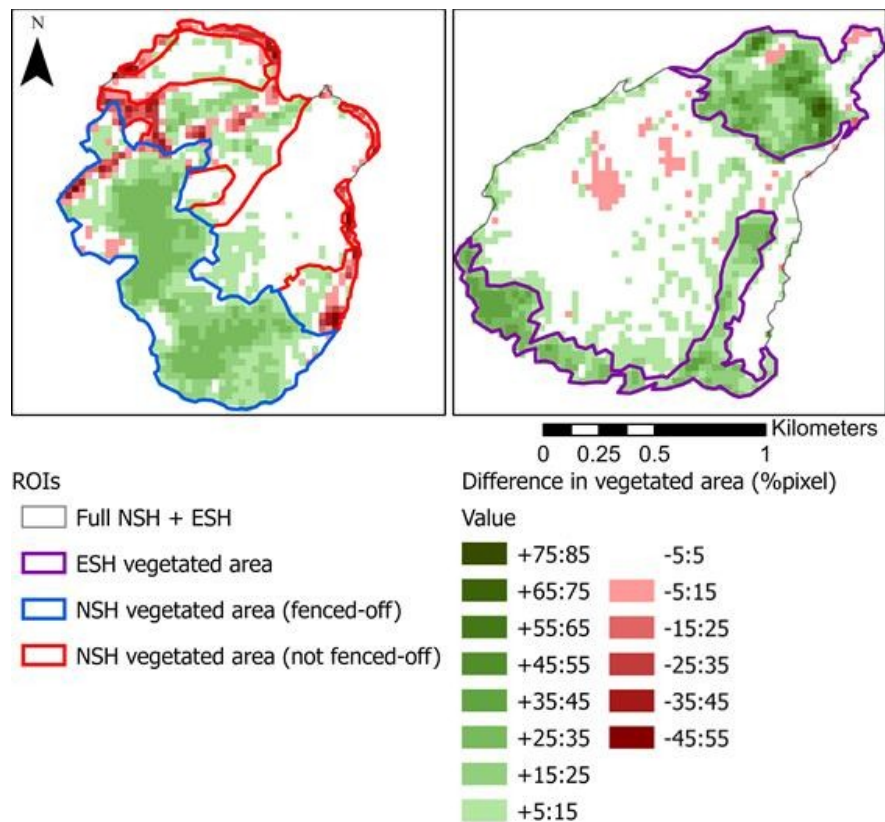


**Fig. 11.** Difference of the classified rasters from June 2018 and June 1984 for North Sand Hills (left) and East Sand Hills (right). Values represent the difference in percent area classified as vegetation for each pixel.

of the western part of the area has lost vegetation where a road, although fenced on either side, has eroded along its margins. The vegetated area open to OHV use has experienced losses in vegetative cover, especially along its margins. Most notably, the eastern margin adjacent to North Sand Creek has experienced loss. Vegetative cover losses on the North Sand Hills dunefield in places exceed 45% of the pixel area, and gains are no greater than 35% of the pixel area.

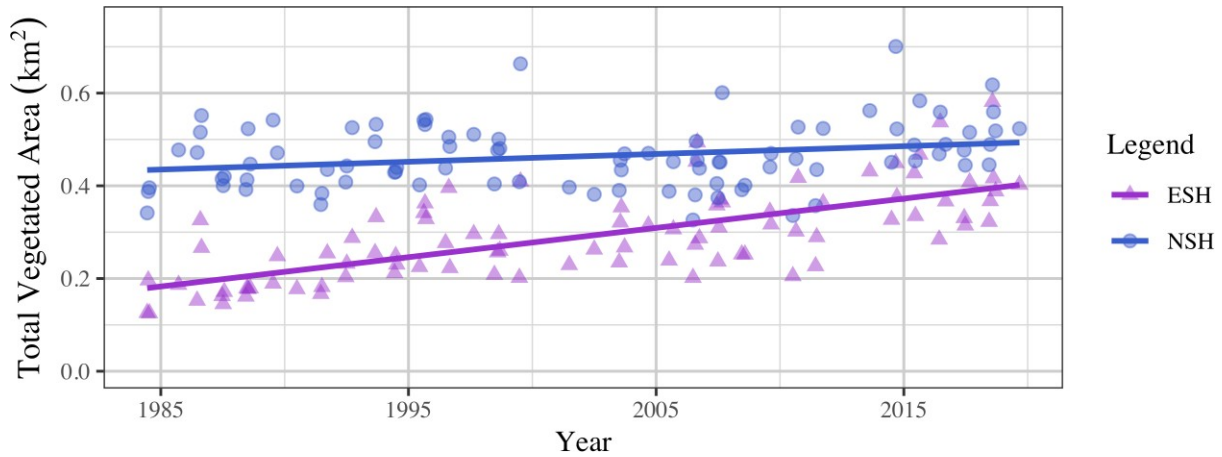


**Fig. 12.** Values and fitted regression lines for the total estimated vegetated area within East Sand Hills (ESH) and North Sand Hills (NSH)

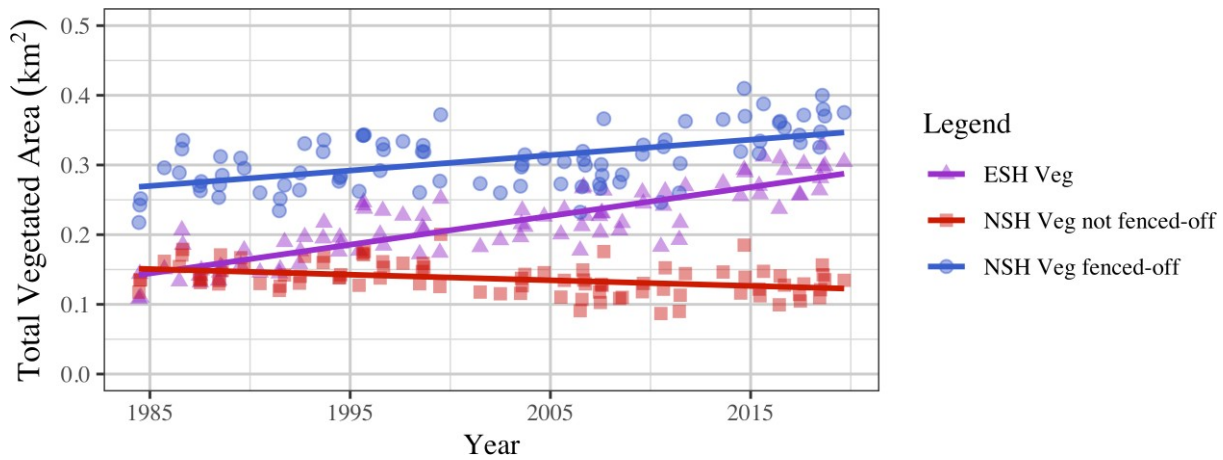


**Fig. 13.** Values and fitted regression lines for total estimated vegetated area within vegetated areas on East Sand Hills (ESH) and North Sand Hills (NSH), with areas on NSH split into areas fenced-off to OHV users, and those not fenced-off

Both ANCOVA models regressing total sand area over time yielded significantly different trends for all regions of interest. Results indicate that both the East Sand Hills and North Sand Hills dunefields have gained vegetative cover at a rate of approximately 6,321 m<sup>2</sup>/year and 1,681 m<sup>2</sup>/year, respectively (Fig. 12). East Sand Hills has gained vegetative cover at a significantly greater rate, with p-value <0.001. The adjusted R<sup>2</sup> of the model is 0.97, indicating good fit, and is highly significant with a p-value <0.001. The model comparing sand cover trends over time for

vegetated areas only indicates that the East Sand Hills vegetated areas have gained vegetative cover at a rate of 4,128 m<sup>2</sup>/year, the fenced-off North Sand Hills vegetated areas have gained vegetative cover at a rate of 2,215 m<sup>2</sup>/year, and the non-fenced vegetated areas have lost vegetative cover at a rate of 805 m<sup>2</sup>/year (Fig. 13). All of these slopes are significantly different with p-values <0.001. This model also has good fit, with an adjusted R<sup>2</sup> of 0.99, and is highly significant with a p-value <0.001.

The statistical analysis checking for seasonal bias in the remote sensing time series data indicates that while the area of vegetation on both dunefields is affected by the time of year at which the image was collected, there is no trend throughout the study period in the time of year of image collection. The model results indicate that day number is a significant predictor for total vegetated area on both North Sand Hills and East Sand Hills (p-values both <0.001). However, the R<sup>2</sup> values for both of these models are low (0.12 and 0.26, respectively), meaning that day number only explains a small portion of the variance in the data. The model regressing day number against year yields insignificant results, with a p-value of 0.59 and R<sup>2</sup> of 0.00. These model results suggest that the time series analyses could have been skewed had the time of year not been randomly distributed across years; however, as the time of year is randomly distributed, the estimated trends of vegetation coverage over time are not affected by seasonal bias.

### *3.2 General Field Observations*

A few general observations of how the two dunefields and creeks differ should be noted before specific results are presented. When I first visited North Sand Creek in November of 2018, I observed the downstream zone to be primarily gravel- and cobble-bedded with a sand bed only in logjam backwater areas. When I visited the creek again on 23 May 2019, the channel had already transformed to completely sand-bedded with antidunes throughout the study area, beginning at the

top of the dunefield and continuing 6 km downstream to State Line Ranch. A game camera in the downstream zone channel captured the channel becoming turbid with mobile sand on May 19. This indicates that the downstream zone aggraded at a rapid rate over the course of the four days between 19 and 23 May. By the time I first visited East Sand Creek on 4 June, the channel bed was a diverse mix of sand, gravel, and cobbles, and remained so throughout the summer.

North Sand Creek exhibited antidunes that migrated upstream in at least some areas until August. Antidunes were never observed in East Sand Creek. The presence of antidunes is controlled by the presence of a sand bed that is at least as deep as the wave amplitude and a Froude number greater than 1, indicating supercritical flow. The Froude number is calculated as follows:

$$F = \frac{V}{\sqrt{gd}} \quad (1)$$

where  $F$  is the Froude number,  $V$  is mean flow velocity,  $g$  is acceleration due to gravity, and  $d$  is flow depth. North Sand Creek therefore has some combination of deeper sand, higher flow velocity, and lower flow depth than East Sand Creek. Given the assumption that East Sand Creek has both higher flow velocity and flow depth due to its larger drainage area, North Sand Creek likely has a consistently deeper sand bed than East Sand Creek.

Although not quantified in this study, the North Sand Hills and East Sand Hills dunes exhibited clear qualitative differences possibly related to OHV impact (Fig. 14). The East Sand Hills dune area is almost entirely covered with sparse grass and shrubs, while the North Sand Hills dune area is almost entirely bare. Additionally, along the North Sand Creek dune-creek interface, I observed widespread evidence for recent vegetation disturbance and gravitational slumping, while I observed no evidence for either along the East Sand Creek dune-creek interface.

Another important difference between the two creeks is that the North Sand Creek tributary is partly ephemeral. Sections of the creek were dry beginning in mid-July and continued dry

through November of 2019. East Sand Creek, on the other hand, was never dry in any section. This difference is likely due to a combination of the North Sand Creek tributary's smaller drainage area, as well as higher eolian influx burying the channel and reducing surface flow.

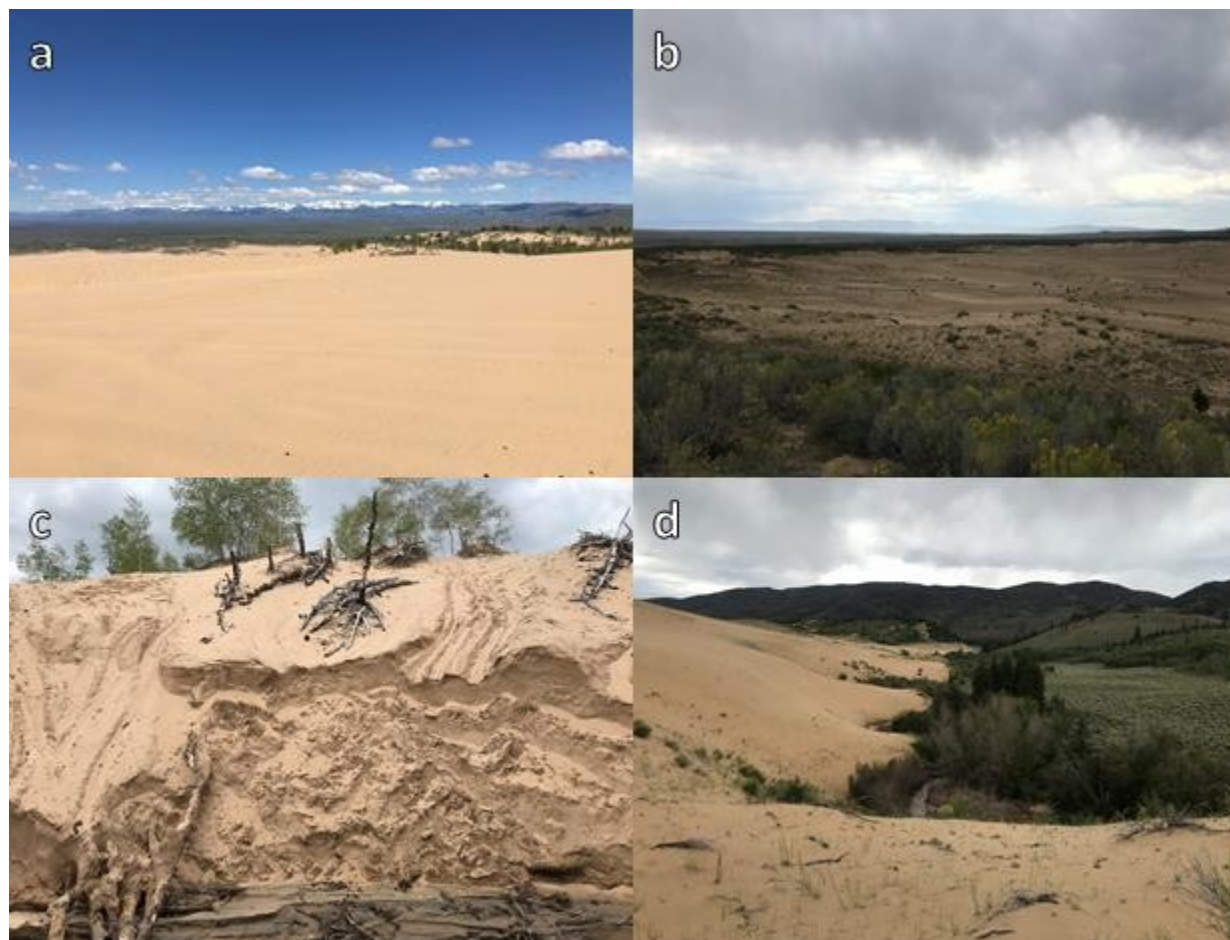


**Fig. 14.** Qualitative comparison of the sand dunes on (a) North Sand Hills and (b) East Sand Hills, and the dune-creek interface at (c) North Sand Creek and (d) East Sand Creek. All photos were taken in the summer of 2019.

### *3.3 Repeat Photography*

The repeat photography analysis reveals clear differences between the two creeks. See Figure 15 and 16 for highlighted repeat photos, Table 2 for a summary of conclusions drawn from the repeat photos, and Appendix A for the photos and more-detailed observations. All five repeat photo locations in the upstream zone of the North Sand Creek tributary exhibited evidence of

recent incision throughout the summer months of May-July, including over-steepened sand banks, channel bed elevation lowering, and formation of SASs. By far the most dramatic change took place at location NP6, where the channel incised >2 vertical meters of sand during the first two weeks of June, leaving behind an SAS. Three out of five of these locations manifested aggradation later in the summer and throughout the autumn, likely due to increased eolian sand influx and declining stream power. Evidence included channel bed material fining and bed elevation rise. The other two locations did not exhibit any notable changes in channel morphology during the late summer and autumn. Neither of the two repeat photo locations in the downstream zone exhibited dramatic change. One transitioned from completely sand-bedded to a mixed bed of sand, gravel, and cobbles during the late summer, indicating some incision, although this was not accompanied by over-steepened sand banks or SAS formation.

**Table 2.** Summary of changes in channel morphology throughout the study period at the 7 repeat photo locations in (a) North Sand Creek and (b) East Sand Creek. Generalized changes are coded as evidence for recent incision (I), aggradation (A), or no change (NC).

(a) North Sand Creek	ID	May-July	August-November	(b) East Sand Creek	ID	May-July	August-November
Upstream Zone	NP8	I	A	Upstream Zone	EP7	NC	NC
	NP7	I	A		EP6	I	NC
	NP6	I	NC		EP5	NC	NC
	NP5	I	NC	Downstream Zone	EP4	NC	NC
	NP3	I	A		EP3	NC	NC
Downstream Zone	NP2	NC	NC		EP2	NC	I
	NP1	NC	I		EP1	NC	NC

The repeat photo locations at East Sand Creek, on the other hand, did not exhibit much notable change throughout the study period. One of the three locations in the upstream zone (EP6) incised in the early summer, as evidenced by the presence of an SAS < 1 m in height, and one of the four locations in the downstream zone incised in the late summer, as evidenced by a transition in bed material from complete sand to mixed sand-cobble-gravel.



**Fig. 15.** Selected repeat photos demonstrate rapid incision and the formation of SASs during the early summer in North Sand Creek locations NP6 and NP3, and the collapse of an SAS at East Sand Creek location EP6.



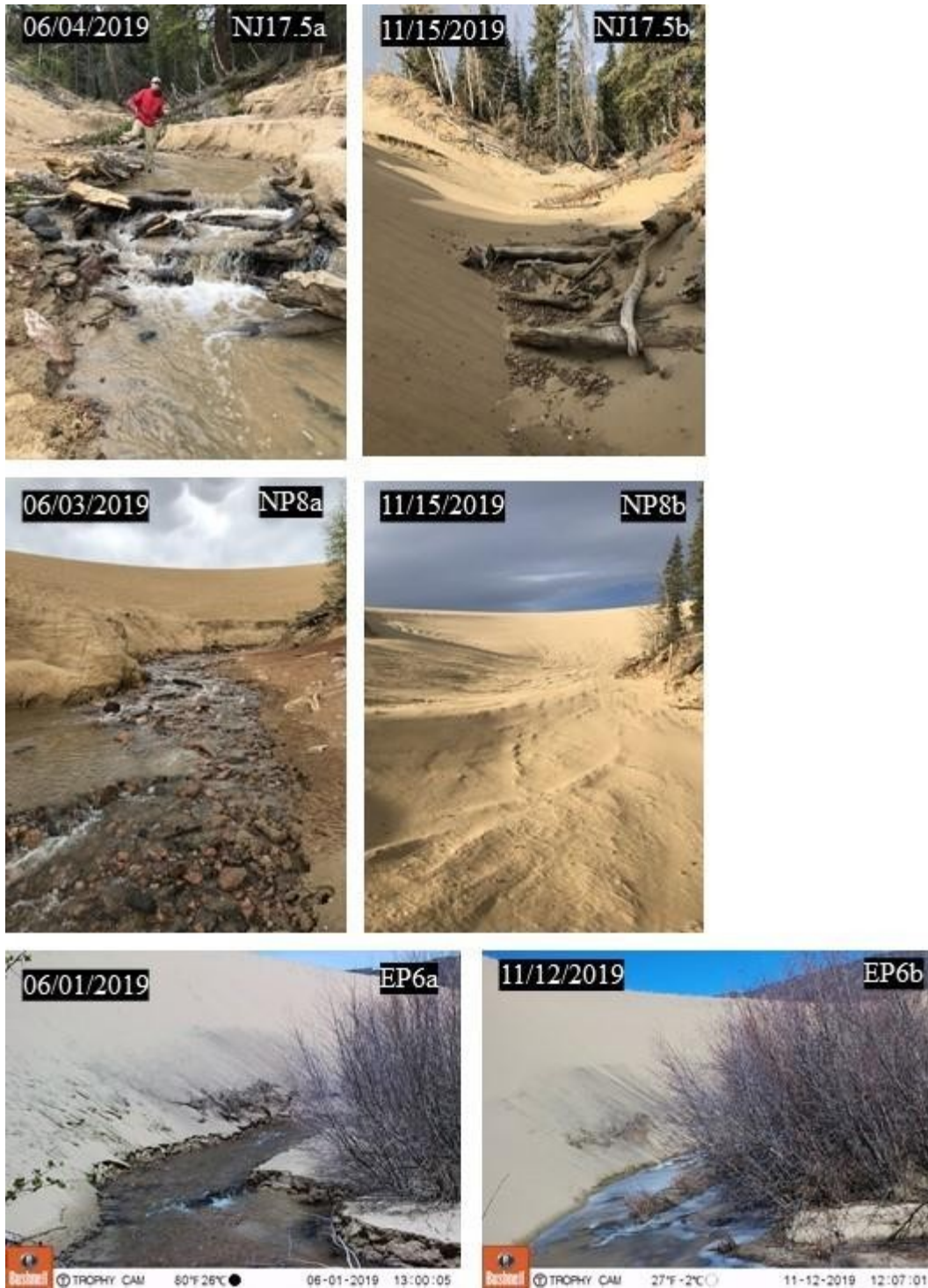


**Fig. 16.** Selected repeat photos demonstrate aggradation during the late summer and autumn at North Sand Creek logjam NJ17.5 and location NP8. Ripples perpendicular to the flow direction, indicating eolian transport, were observed at both locations when the November photos were taken. A similar location in East Sand Creek (EP6) did not demonstrate aggradation.

The repeat photography results indicate that over the course of the summer of 2019, North Sand Creek incised a high volume of sand in the upstream zone, that passed through, rather than being deposited in, the downstream zone. This indicates the presence of a highly translative sediment wave passing through the area of the channel outside of the logjam backwater, corresponding with transport model a or c in the conceptual model (Fig. 2; Table 1). East Sand Creek, on the other hand, experienced only scattered and low-magnitude incision with no clear longitudinal pattern, which corresponds best with the null model, transport model 0, corresponding with no sediment wave.

### *3.4 SAS measurements*

The SAS measurements also reveal clear differences between the creeks (Table 3). North Sand Creek had two distinct SASs, one each in the upstream and downstream zone, which were both observed to persist during the weeks of 12 June and 6 August. The SAS in the upstream zone (NS2) was a maximum of 840 m long in August, at its widest point 34.3 m wide, and at its deepest point 5.3 m deep. The repeat photography illustrates that flow in the creek's upstream zone began during the week of 13 May, yielding the inference that the creek incised an estimated 6096 m<sup>3</sup> of sand from the upstream zone over the course of its first month of flow, and a further 3524 m<sup>3</sup> during the next 2 months. The SAS in the downstream zone (NS1) was smaller than NS2. This SAS was a maximum length of 180 m in August, with a maximum width of 16.2 m and depth of 1.2 m. These measurements yielded incised sand volume estimates of 53 and 59 m<sup>3</sup> for June and August, respectively, indicating that the creek continued to incise a relatively small volume of sand from the downstream zone during the late summer months.

The SASs measured in East Sand Creek were notably different from those in North Sand Creek. Seven SASs were observed in the creek in June. By August, all but one of these had been

destroyed, while six new SASs had formed. All of these SASs were much smaller than those observed at North Sand Creek. The largest SAS (ES10) was observed in August, with a length of 40 m, maximum width of 5.4 m, maximum height of 0.8 m, and a total volume estimate of 6 m<sup>3</sup>—notably three orders of magnitude smaller than the largest SAS of North Sand Creek. The total estimated incised sand volume was higher in the upstream zone than the downstream zone for both June and August. The total ISV increased by 3 m<sup>3</sup> in the upstream zone over the course of the summer but decreased by 3 m<sup>3</sup> in the downstream zone.

**Table 3.** Estimates of incised sand volume (ISV) for each SAS measured in (a) North Sand Creek and (b) East Sand Creek, and also totaled by zone. See Appendix Section 2 for complete measured SAS data and Figure 3 for a map of SAS locations.

(a) North Sand Creek	ID	June ISV (m <sup>3</sup> )	Aug. ISV (m <sup>3</sup> )	Net Change (m <sup>3</sup> )
Upstream Zone	NS2/ <b>Total</b>	<b>6096</b>	<b>9620</b>	<b>+3524</b>
Downstream Zone	NS1/ <b>Total</b>	<b>53</b>	<b>59</b>	<b>+6</b>

(b) East Sand Creek	ID	June ISV (m <sup>3</sup> )	Aug. ISV (m <sup>3</sup> )	Net Change (m <sup>3</sup> )
Upstream Zone	ES12	0	0.6	+0.6
	ES11	0	4.0	+4.0
	ES10	0	5.9	+5.9
	ES9	0.1	0	--
	ES8	0.3	3.5	+3.2
	ES7	10.7	0	--
	<b>Total</b>	<b>11</b>	<b>14</b>	<b>+3</b>
Downstream Zone	ES6	1.3	0	--
	ES5	0	1.8	+1.8
	ES4	0	2.0	+2.0
	ES3	1.4	0	--
	ES2	3.1	0	--
	ES1	2.1	0	--
	<b>Total</b>	<b>7</b>	<b>4</b>	<b>-3</b>

The SAS results mirror the repeat photography results, in more quantitative terms. They also indicate that North Sand Creek incised a high volume of sand in the upstream zone, that passed through, rather than being deposited in, the downstream zone. This indicates the presence of a

highly translative sediment wave passing through the area of the channel outside the logjam backwater, corresponding with transport model a or c in the conceptual model (Fig. 2; Table 1). East Sand Creek, on the other hand, experienced only scattered and low-magnitude incision with no clear longitudinal pattern, which corresponds best with the null model, transport model 0, corresponding with no sediment wave.

### *3.5 Logjam sand wedge measurements*

The logjam sand wedge measurement analysis revealed that logjams at North Sand Creek stored more sand overall than those at East Sand Creek (Table 4; Fig. 17; Fig. 18). For example, upon first measurement, the total logjam sand storage at North Sand Creek was estimated to be 5061 m<sup>3</sup>, compared to 611 m<sup>3</sup> at East Sand Creek. Despite this order-of-magnitude difference in total sand storage volume, the logjam sand wedges in the two creeks shared many similarities. Each creek had one logjam storing a disproportionately large volume of sand compared to the others. Upon first measurement, logjam NJ16 in North Sand Creek was estimated to store 3012 m<sup>3</sup> of sand, 60% of the creek's total, while EJ10 at East Sand Creek stored 57 m<sup>3</sup> of sand, 51% of the total. Both of these logjams were located near the bottom of the upstream zone in their respective creek. Other than the relative position of the logjam with the highest sand storage, there are no other obvious longitudinal trends in sand wedge depth, length, or estimated volume in either creek (Fig. 17; Fig. 18). When totaled by zone, the upstream zone logjams stored more sand than the downstream logjams, and in total both zones lost sand over time. Most logjams at North Sand Creek had a net loss of sand over time (19 out of 20), although only approximately half lost sand at East Sand Creek (14 out of 25) (Table 4).

**Table 4.** The initial, final, and net change in logjam sand wedge storage for all logjams throughout the study period.

(a) North Sand Creek	ID	Initial V (m <sup>3</sup> )	Final V (m <sup>3</sup> )	Net Change (m <sup>3</sup> )
Upstream Zone	NJ19	4.6	3.3	-1.4
	NJ18	572.4	51.0	-521.4
	NJ17.5	5.7	8.3	+2.6
	NJ17	182.4	36.0	-146.4
	NJ16	3011.8	1565.2	-1446.6
	<b>Total</b>	<b>3777</b>	<b>1664</b>	<b>-2113</b>
Downstream Zone	NJ15	1.6	1.5	0.0
	NJ14	1.2	0.7	-0.5
	NJ13	3.5	0.0	-3.5
	NJ11.5	4.1	0.6	-3.5
	NJ11	4.4	0.3	-4.1
	NJ10	0.5	0.0	-0.5
	NJ9	2.3	0.3	-2.0
	NJ8	1.0	0.0	-1.0
	NJ7	446.9	1.3	-445.6
	NJ6	48.9	44.1	-4.8
	NJ5	61.2	4.0	-57.2
	NJ4	27.7	6.5	-21.1
	NJ3	218.8	0.0	-218.8
	NJ2	440.2	0.0	-440.2
	NJ1	22.3	13.5	-8.8
<b>Total</b>	<b>1285</b>	<b>73</b>	<b>-1212</b>	

(b) East Sand Creek	ID	Initial V (m <sup>3</sup> )	Final V (m <sup>3</sup> )	Net Change (m <sup>3</sup> )
Upstream Zone	EJ26	1.33	0.0	-1.3
	EJ25	3.1	0.1	-3.0
	EJ24	2.7	3.0	+0.2
	EJ22	1.9	4.3	+2.4
	EJ21	1.0	0.2	-0.8
	EJ20	1.1	0.3	-0.7
	EJ19	0.9	1.3	+0.4
	EJ18	6.7	7.6	+0.9
	EJ17	12.2	90.3	+78.1
	EJ16	5.6	0.0	-5.6
	EJ15.5	10.7	0.0	-10.7
	EJ14	0.2	5.1	+5.0
	EJ13	30.7	8.6	-22.1
	EJ12	71.3	1.6	-69.7
	EJ11	1.4	92.8	+91.4
	EJ10	56.5	13.8	-42.7
EJ9	311.9	182.5	-129.3	

	EJ8	4.5	2.1	-2.3
	<b>Total</b>	<b>523</b>	<b>414</b>	<b>-110</b>
Downstream Zone	EJ7.5	9.8	2.7	-7.1
	EJ7	11.8	18.0	+6.3
	EJ6	0.0	0.0	0.0
	EJ5	4.0	3.8	-0.2
	EJ4	0.0	12.3	+12.3
	EJ3	8.2	11.9	+3.7
	EJ2	47.3	10.9	-36.4
	EJ1	6.8	13.4	+6.6
	<b>Total</b>	<b>92</b>	<b>75</b>	<b>-17</b>

### North Sand Creek

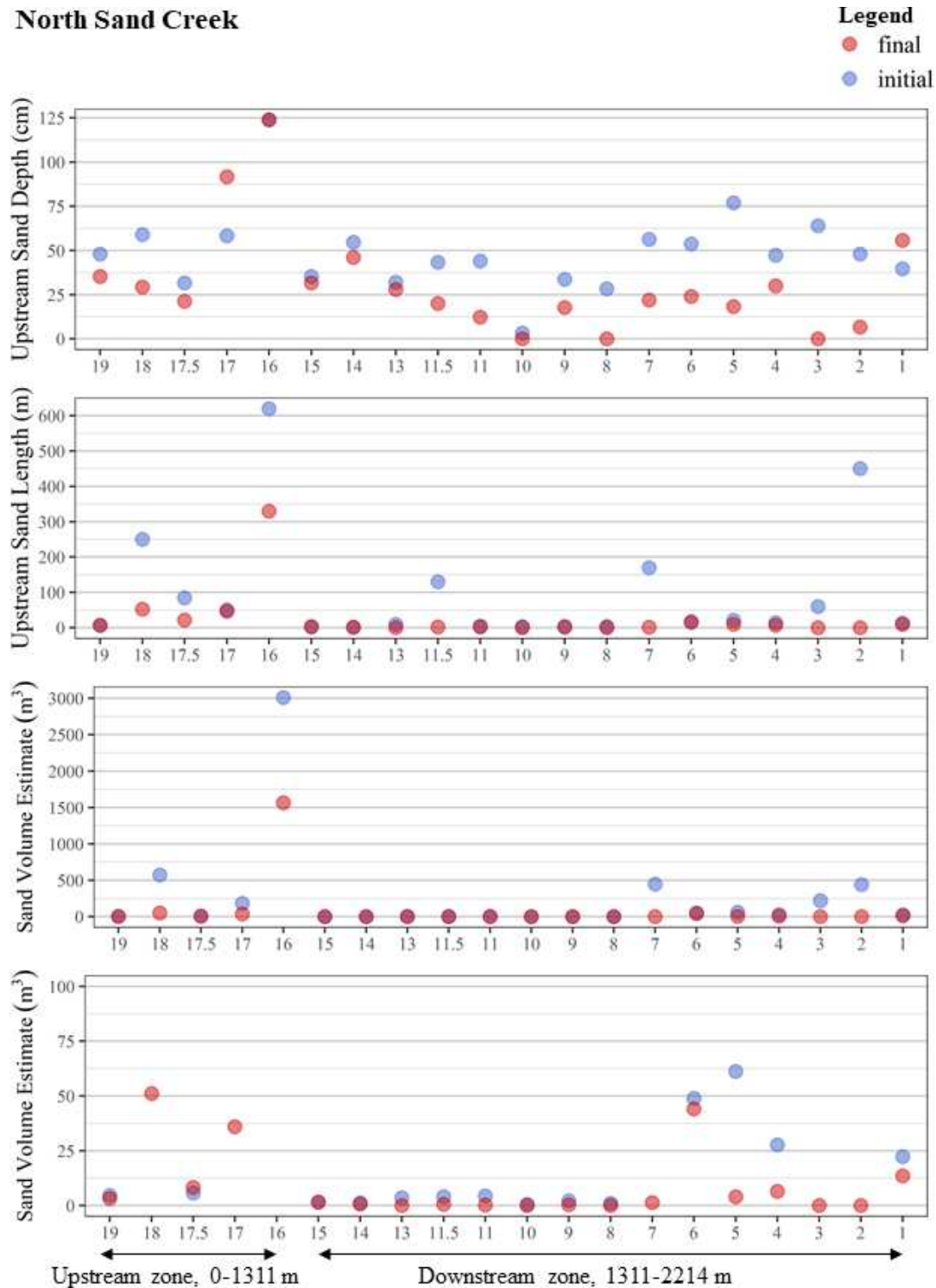


**Fig. 17.** Initial and final measurements for sand wedge upstream sand depth, upstream sand length, and estimated volume for all logjams in North Sand Creek. Logjam ID number is represented on the x axis. Volume is represented on axis representing the full range of measurements, as on a y-axis maximum of 100 m<sup>3</sup> to make data from smaller sand wedges visible.

### East Sand Creek

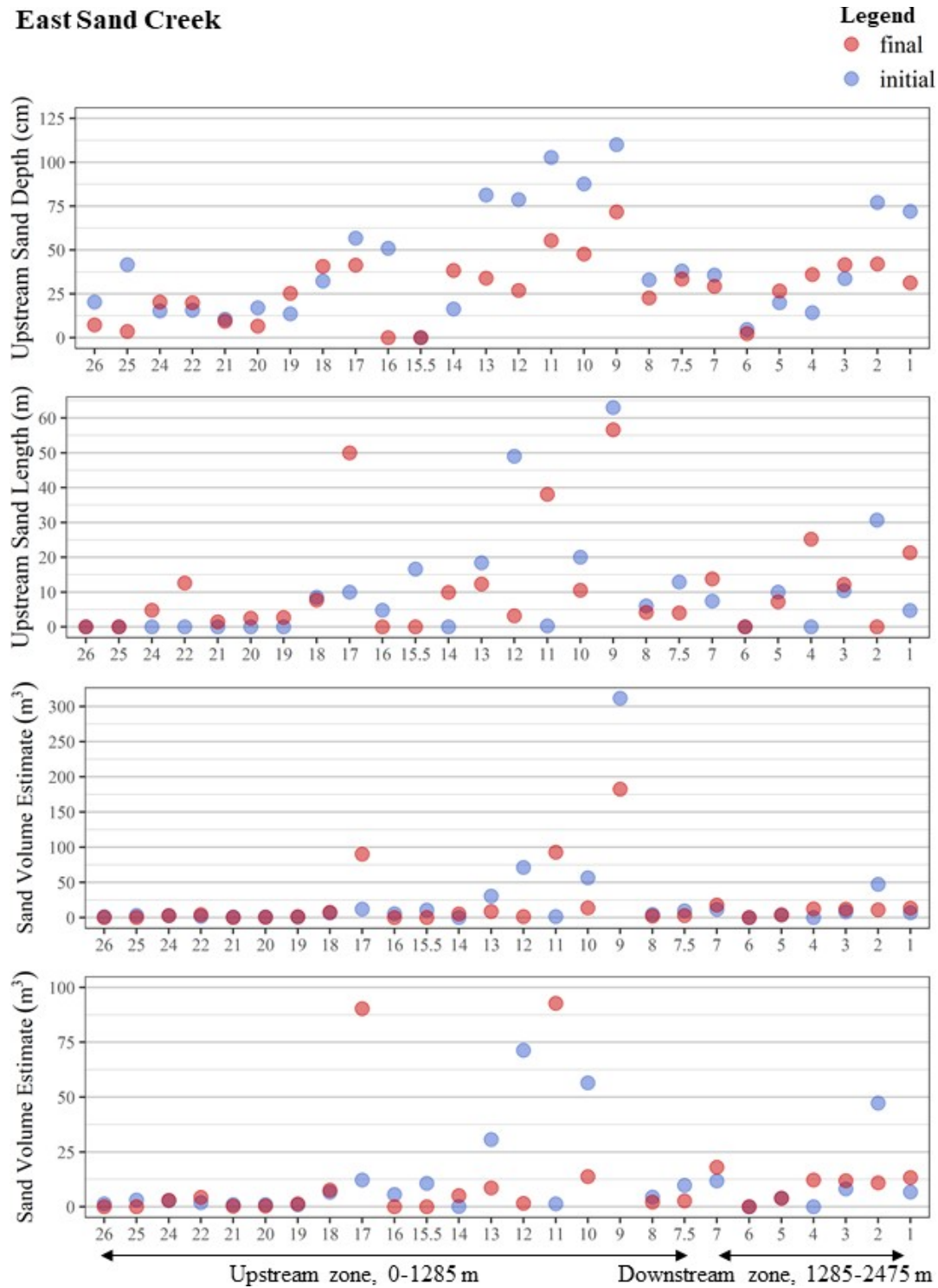


**Fig. 18.** Initial and final measurements for sand wedge upstream sand depth, upstream sand length, and estimated volume for all logjams in East Sand Creek. Logjam ID number is represented on the x axis. Volume is represented on axis representing the full range of measurements, as on a y-axis maximum of 100 m<sup>3</sup> to make data from smaller sand wedges visible.



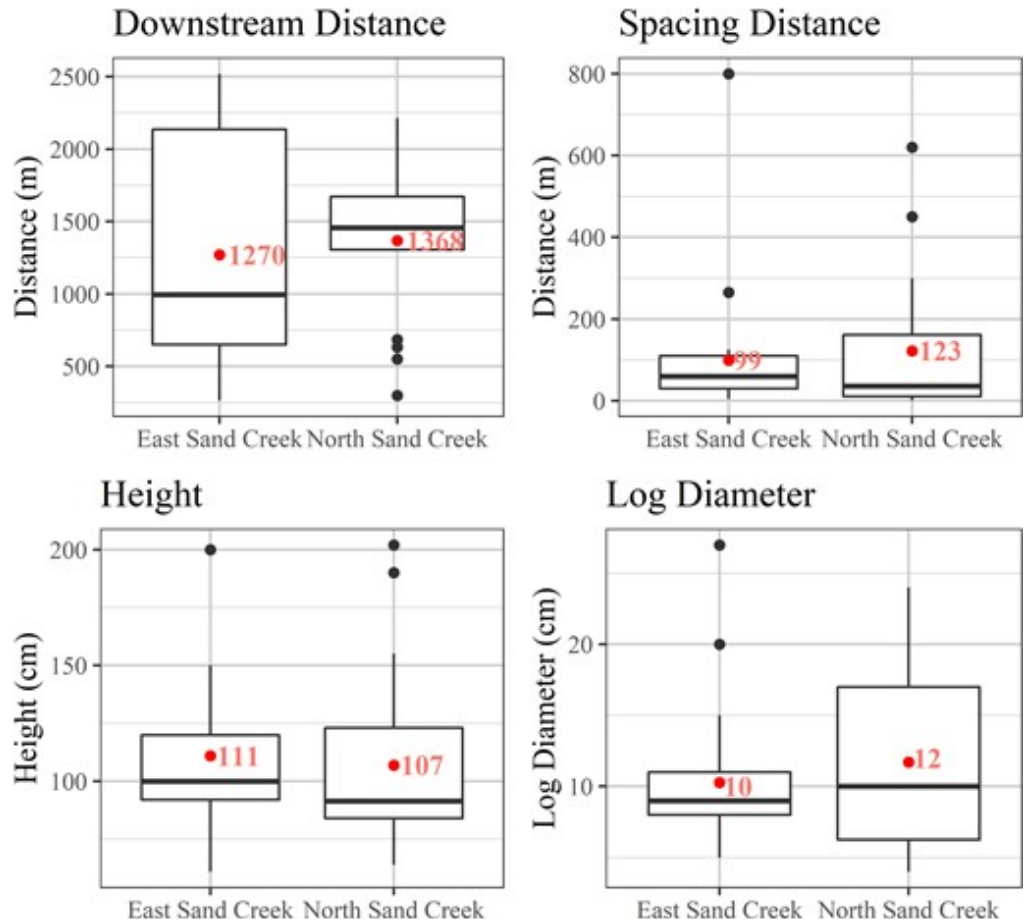


**Fig. 19.** Box-and-whisker plots of four variables potentially associated with storage volume: (a) downstream distance, (b) spacing distance, (c) logjam height, and (d) largest log diameter. Horizontal lines represent the data median; labeled red points represent the mean; boxes represent the range of the first and third quartile; whiskers represent the range of the first and fourth quartile; and points represent potential outliers.

## MANOVA

The MANOVA test of the four measured variables potentially associated with a logjam’s sand storage capacity—distance downstream, spacing distance, height, and largest log diameter (Fig. 19)—returned a p-value of 0.828, indicating failure to reject the null hypothesis that there is a difference between the means in any of these variables between the two creeks. This suggests that differences in logjam sand storage between the creeks are driven by differences in sediment transport dynamics rather than by characteristics of the logjams.

Regression of zone total sand wedge volume over time

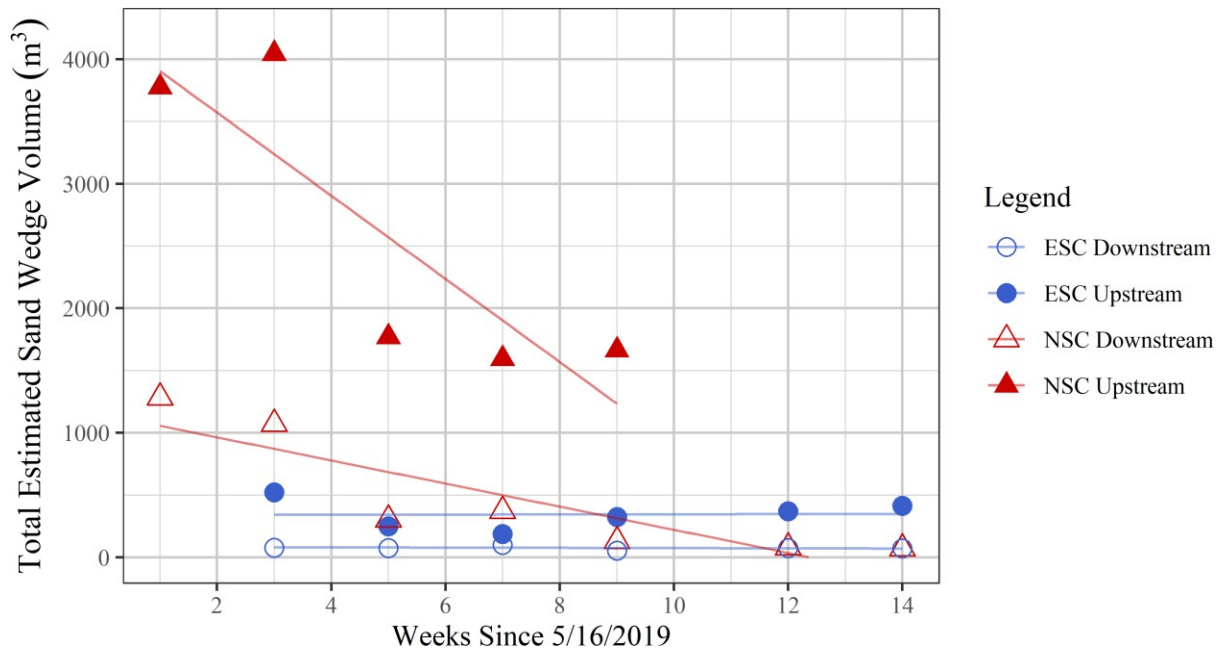


**Fig. 20.** Values (points) and fitted regression lines for the total logjam sand wedge storage over time for each zone.

**Table 5.** Coefficients and diagnostics for the ANCOVA model regressing total logjam sand wedge volume over time with site and zone as a covariate. The p-value column corresponds to the test of the coefficient against 0.

Model Results	Model Term	Estimate	p-value
ESC Upstream Zone	Intercept	340 m <sup>3</sup>	0.3407
	Slope	+0.564 m <sup>3</sup> /week	0.9883
ESC Downstream Zone	Intercept	84 m <sup>3</sup>	0.8111
	Slope	-0.944 m <sup>3</sup> /week	0.9804
NSC Upstream Zone	Intercept	4238 m <sup>3</sup>	<0.0001
	Slope	-334 m <sup>3</sup> /week	<0.0001
NSC Downstream Zone	Intercept	1150 m <sup>3</sup>	0.0004
	Slope	-93 m <sup>3</sup> /week	0.0079
Model Diagnostics	R <sup>2</sup> (adjusted)	0.930	<0.0001

The model results of the regression of zone total logjam sand wedge storage over time generally reveal trends at North Sand Creek to be significant, and those at East Sand Creek to be not significant (Fig. 20). The model was overall significant with a p-value of  $3 \times 10^{-9}$  and R<sup>2</sup> of 0.930 (Table 5). The model estimated the slopes of the North Sand Creek upstream zone and

downstream zone regression at -334 and -93 m<sup>3</sup>/week, respectively. Both of these values were significantly less than 0, with respective p-values of <0.001 and 0.008. The slope corresponding to the upstream zone was also significantly more negative than that of the downstream zone, with a p-value of 0.008. The slopes of the East Sand Creek upstream zone and downstream zone regression were +0.564 and -0.944 m<sup>3</sup>/week, respectively, neither of which were significantly different from 0 (respective p-values, 0.989 and 0.980), or from each other (p-value, 1.000).

Because logjams in both the North Sand Creek upstream and downstream zones lost sand at a rate significantly less than 0, but at a significantly more negative rate in the upstream zone, we can conclude that sand does translate through the logjam backwater area, but attenuates as it translates. Combined with the results from the repeat photography and SAS analyses, this indicates the presence of a highly translative sediment wave that is attenuated by logjams, corresponding to transport model c in the conceptual model (Fig. 2; Table 1). Because the trends of logjam sand storage over time in the upstream and downstream zones of East Sand Creek are not significantly different from 0 or each other, we can conclude that sand does not translate through the logjam backwater area. Combined with the results from repeat photography and SAS measurements, this also points to the null model, or no sediment wave, in East Sand Creek.

#### Regressions of measured variables against time at individual logjams

The regressions of the “response” variables of logjam sand wedges—upstream sand wedge depth, length, and estimated volume—revealed some similarity among the logjams of the creeks in terms of trends in sand wedge depth, but differences in terms of sand wedge length and estimated volume (Table 6; Table 7). Both creeks had several logjams with significantly negative trends in upstream sand depth at the  $\alpha=0.1$  level; 6 out of 20 at North Sand Creek, and 6 out of 26 at East Sand Creek. About ¼ of the logjams in both creeks, therefore, experienced sand wedge lowering

throughout the summer. However, the creeks do exhibit differences in trends of sand wedge length and volume. Five out of 20 of the logjams at North Sand Creek had significant negative trends in sand wedge length, while only 1 out of 26 of the logjams at East Sand Creek had a significant trend and it was positive. More logjams in North Sand Creek therefore experienced sand wedge shortening than those in East Sand Creek. Of the three logjams in both creeks that had significant negative trends in volume over time—NJ18, NJ16, and NJ7—all three had significantly negative trends in upstream length, but only one had a significantly negative trend in depth. This suggests that overall changes in logjam sand storage are driven by sand wedge shortening rather than lowering, and that logjams that are farther apart lose sand more quickly.

**Table 6.** Model results for the regression of logjam sand wedge storage over time at all logjams individually. Values marked with a “\*\*\*” are significantly different from 0 at the  $\alpha=0.05$  level, and those marked with a “\*” are significant at  $\alpha=0.1$ .

(a) North Sand Creek	ID	U Depth Trend Est. (cm/week)	UL Trend Est. (cm/week)	V Trend Est. (m <sup>3</sup> /week)
Upstream Zone	NJ19	-1.8	-12.0	-0.2
	NJ18	-2.3	-1124.5**	-21.6*
	NJ17.5	-0.3	-130.8	-4.4
	NJ17	+1.8	-74.9	+0.4
	NJ16	N/A	-4350**	-252.7**
Downstream Zone	NJ15	-1.5	0.0	-0.1
	NJ14	-0.3	-1.0	0.0
	NJ13	+1.25	-96.0	-0.2
	NJ11.5	-3.5**	-560.9	-0.7
	NJ11	-3.4**	-14.8	-5.8
	NJ10	+3.2	0.0	+0.1
	NJ9	-0.7	-22.4	-0.2
	NJ8	-0.5	0.0	0.0
	NJ7	-2.2**	-1326.3**	-26.0*
	NJ6	-2.0*	+7.5	-0.8
	NJ5	-3.4**	-97.8	-4.4
	NJ4	-0.5	-66.5	-1.3
	NJ3	-4.8**	-454.9**	-15.2
	NJ2	-2.7**	-4233.6**	-15.2
NJ1	-0.1	-8.0	-0.1	

<b>(b) East Sand Creek</b>	<b>ID</b>	<b>U Depth Trend Est. (cm/week)</b>	<b>UL Trend Est. (cm/week)</b>	<b>V Trend Est. (m<sup>3</sup>/week)</b>
Upstream Zone	EJ26	-0.3	0.0	-0.1
	EJ25	-2.6*	+29.4	-0.1
	EJ24	+1.0	+47.5	+0.1
	EJ22	+0.6	+164.9	+0.4
	EJ21	+0.1	+9.7	-0.1
	EJ20	-0.2	+46.5	0.0
	EJ19	+2.1	+30.5	+0.1
	EJ18	+1.1	+34.2	+0.3
	EJ17	-0.9	+474.5*	+7.6
	EJ16	-4.9**	-53.1	-0.5
	EJ15.5	-2.6	-186.8	-1.2
	EJ14	+2.7**	+177.9	+0.8
	EJ13	-4.9	-46.6	-1.9
	EJ12	-4.7**	-409.2	-5.7
	EJ11	-2.7**	+396.4	+10.5
	EJ10	-1.6	+2.7	-2.0
	EJ9	-1.9	-57.3	-7.7
	EJ8	-1.4	+31.4	-0.1
Downstream Zone	EJ7.5	-1.0	-102.6	+0.4
	EJ7	-1.9	+111.0	-1.0
	EJ6	0.0	0.0	0.0
	EJ5	-0.2	+3.4	0.0
	EJ4	+2.1	+241.9	+1.2
	EJ3	-0.6	+29.6	0.0
	EJ2	-4.4**	-303.1	-3.7
	EJ1	-3.7*	+195.9	+1.1

**Table 7.** Model diagnostics for the three models of trends in upstream sand depth, upstream sand length, and estimated volume at all logjams individually.

<b>Model</b>	<b>R<sup>2</sup> (adjusted)</b>	<b>p-value</b>
U Depth	0.896	<0.0001
UL	0.913	<0.0001
V	0.896	<0.0001

## 4. Discussion

### 4.1 Land Cover Trends Over Time

The remote sensing analysis results indicate that, contrary to the first hypothesis, both dunefields as a whole have gained vegetative cover since 1984. The rate of gain of vegetative cover is significantly less at North Sand Hills, however, indicating that impacts from OHV recreation may be responsible for reduced gains. The underlying causes of this decadal-scale land cover trend are unknown, but it could represent a slow recovery to some pre-1984 disturbance, such as wildfire, grazing pressure, or drought, or the response of the ecosystem to decadal-scale climate change.

The slower rate of vegetation coverage increase on North Sand Hills is likely due to the effect of OHV recreation, but there may be some other differences in the dunefields affecting rates of change. If both the dunefields experienced some disturbance prior to 1984 that they are recovering from, the disturbance may have been of a different nature or magnitude between the dunefields, resulting in different responses from vegetation. Also, North Sand Hills is ~120 m higher in elevation than East Sand Hills, which might result in minor differences in vegetation composition, such as more coverage of conifers and aspen, rather than grass and shrubs. These trees, due to longer life cycles and greater need for water, may experience mortality or slowed growth during drought periods, and be slower to recover than grass and shrubs (e.g. Vose et al., 2016).

The contrasting management strategies within the North Sand Hills dunefield allow for a specific analysis of the impact of OHV recreation. North Sand Hills vegetated areas that are not fenced off to OHV users lost vegetative cover at a rate of 805 m<sup>2</sup>/year, which is significantly more negative than the fenced-off vegetated areas. Vegetated areas on North Sand Hills that are fenced-off to OHV users have gained vegetation over time, although at a significantly slower rate than

those on East Sand Hills, indicating a possible continuing impact from elevated eolian transport rates from adjacent unfenced areas.

These results ultimately indicate that fencing off areas on North Sand Hills may reduce, though not eliminate, impact from OHVs. BLM managers have already fenced off more areas of the dunefield than were visible in the 2019 ArcGIS Pro basemap imagery, including the eastern margin adjacent to North Sand Creek. This is a step in the right direction, although more direct action, such as seeding native vegetation and stabilizing areas of open sand, may need to be taken to protect recovering vegetation in disturbed areas.

#### 4.2 Comparison of SAS and logjam sand wedge results

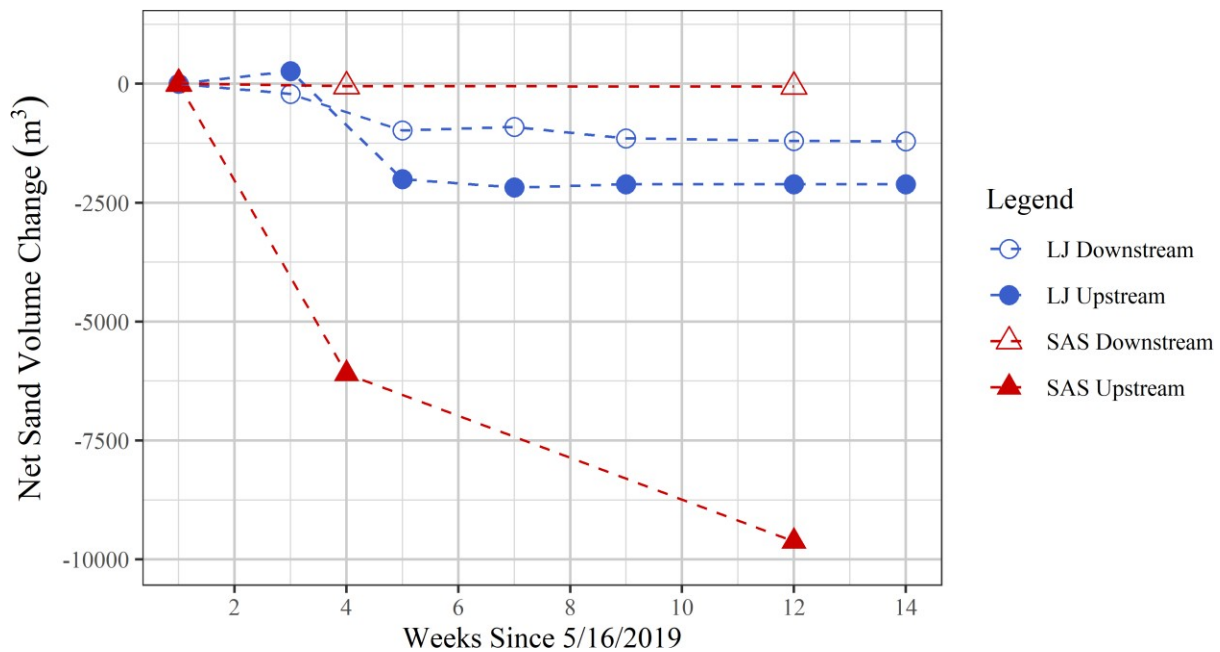


**Fig. 21.** Plot comparing net loss in sand volume over time within logjam sand wedges and within the rest of the channel, as determined from SAS measurements. ISV of SASs were inferred to be 0 on 16 May 2019 (the first week of flow in the upstream zone). Lines in the plot are not fitted regression lines and are meant only to qualitatively compare the approximate rates of sand loss before and after the possible threshold-crossing event between weeks 3 and 4.

Comparison of the results of the North Sand Creek logjam sand wedge and SAS analyses reveal clear differences between sand storage patterns within logjam backwater areas and in the

rest of the channel (Fig. 15). While both areas experienced a net loss of sand, SAS measurements indicate that sand loss in areas outside of the logjam backwater outpaced that of logjam sand wedges throughout the summer of 2019. The disparity between sand storage in the upstream and downstream zones is also far more extreme for areas outside of logjam backwater than for logjam sand wedges. These differences suggest that sand translates rapidly through areas outside of the logjam backwater areas, but is attenuated somewhat by logjams, corresponding with transport model c in the conceptual model (Fig. 2; Table 1).

Another inference from this comparison is the presence of a possible threshold-crossing event with rapid sand transport between 4 June and 11 June 2019. During this week, the channel evidently incised over 2 vertical meters and formed an SAS at the NP6 repeat photo location. Logjam sand storage analysis indicates that most of the net sand loss in both zones occurred during this week—over 2000 m<sup>3</sup> of sand in the upstream zone and 500 m<sup>3</sup> in the downstream (Fig. 20). The SAS measurements also correspond with this timeline. Given that the SASs formed only after flow began in the upstream zone on 16 May, most of the associated incision occurred before the fourth week of flow, followed by a slower rate for the rest of the summer. Although there are not enough data to make a robust comparison, it is clear that the net sand losses both within and outside of the logjam backwater area follow similar trends before and after the possible threshold-crossing event.

The mechanisms associated with this potential sediment transport threshold are unknown but are likely associated with an increase in flow velocity. This increase is likely in part due to the continuing rise in meltwater from the winter snowpack sourced via surface and shallow groundwater pathways. USGS gage data from the North Platte River near Cowdrey, CO indicate that flow in the North Park area generally continued to rise between 16 May and 24 June of 2019



(USGS, 2020c). Additionally, a weather station in Walden, CO recorded 12.7 cm of snowfall and 2.3 cm of rain on 28-29 May. Daily highs during the week of 4 June ranged between 18 and 22 °C (CO CC, 2020), possibly resulting in rapid melt of the recent snow and runoff into North Sand Creek. The incision in North Sand Creek may also have created a positive feedback loop in the early summer, whereby channel narrowing resulted in a lower width:depth ratio, in turn creating elevated flow velocities that promoted further incision.

#### *4.3 Sediment transport model*

First, the MANOVA comparison of variables inferred to be associated with logjam sand storage compacity concluded that there are no significant differences between logjams in the creeks, and we can therefore make valid comparisons in logjam sand storage dynamics between the creeks without accounting for differences in the logjams themselves.

Results indicate that East Sand Creek did not experience a sediment wave in the summer of 2019. Both repeat photos and the presence of scattered, low-magnitude SASs suggest that some incision did occur, although there is no clear temporal or longitudinal pattern. The regression of total logjam sand wedge storage over time indicates that the trends in both zones are not significantly different from 0. The regressions of sand wedge variables over time at individual logjams reveals that some change does take place in logjam storage, with 6 out of 26 logjams having significant negative trends in sand depth, despite a lack of significant negative trends in upstream length or estimated volume. East Sand Creek did transport eolian sand throughout the summer of 2019, but it appears that there likely was not enough eolian influx to initiate a true sediment wave that could be detected with these methods.

In North Sand Creek, on the other hand, results indicate that a highly translative sediment wave occurred, which was also partially attenuated by logjams, corresponding with transport

model c in the conceptual model (Fig. 2; Table 1). This conclusion is supported by the evidence from both repeat photos and SAS measurements of widespread and dramatic incision and aggradation in the upstream zone, coupled with relatively little change in the downstream zone, as well as regression slopes of total zone logjam storage over time which are both negative and significantly different.

Analysis of the repeat photos revealed a clear annual cycle of incision and aggradation in the upstream zone of North Sand Creek. Incision generally occurred during late May and early June. By August, many of the locations in the upstream zone began to experience aggradation, most likely due to the combination of increasing eolian influx from the adjacent sand dunes and decreasing flow. The repeat photo locations in the downstream zone, on the other hand, did not experience dramatic change, although they exhibited evidence for some incision between August and November. The SAS analysis yields similar conclusions as the repeat photos. The SAS in the upstream zone by August represented an impressive incised sand volume of 9620 m<sup>3</sup>. The downstream zone also experienced incision associated with an SAS, although two orders of magnitude smaller.

The regressions of total logjam sand wedge storage by zone over time reveal that within logjam backwater areas, sand moved through both translation and dispersal. Both the upstream and downstream zones had significant negative trends, and the upstream zone had a significantly more negative trend than the downstream zone. Additionally, there is evidence that this change occurred by a reduction in sand wedge length, rather than depth. While 5 out of 20 of the logjams at North Sand Creek did have significantly negative trends in upstream sand depth in the individual logjam regressions—a maximum of -4.9 cm/week—the trends in sand length—a maximum of -21 m/week—ultimately outweighed the effects of depth in the volume estimate. The three logjams

with significant trends in volume also were in the top 20% of highest spacing distance of all logjams in the creek, suggesting that more densely spaced logjams attenuate sediment waves more effectively.

#### *4.4. Management implications*



**Fig. 22.** A buried fence crossing North Sand Creek on State Line Ranch, 5.5 km downstream of the active sand dunes. This photo was taken on 8 August 2019.

Although they differed in magnitude, both the upstream and downstream zones of North Sand Creek appeared to incise synchronously, thus raising the question of where the incised sand is being deposited. The answer may come from observations made on State Line Ranch land, 5.5 km downstream of the active sand dunes. This area was not studied in depth but was visited twice—once in June and once in August—to take photographs and notes on channel morphology. The channel reach near the headgate of the ranch’s irrigation network has clearly aggraded dramatically over the past decade (Fig. 22). Channel widening and aggradation in the irrigation network is evident in aerial imagery beginning in 2009 and expands throughout the network

through 2017 (Fig. 23). It may be that the irrigation network is receiving most or all of the sand incised from the area near the active sand dunes. During the summer of 2019, I measured the amount of sand incised from the upstream zone to be 9600 m<sup>3</sup>—for reference, this is almost the volume of 4 Olympic-sized swimming pools.

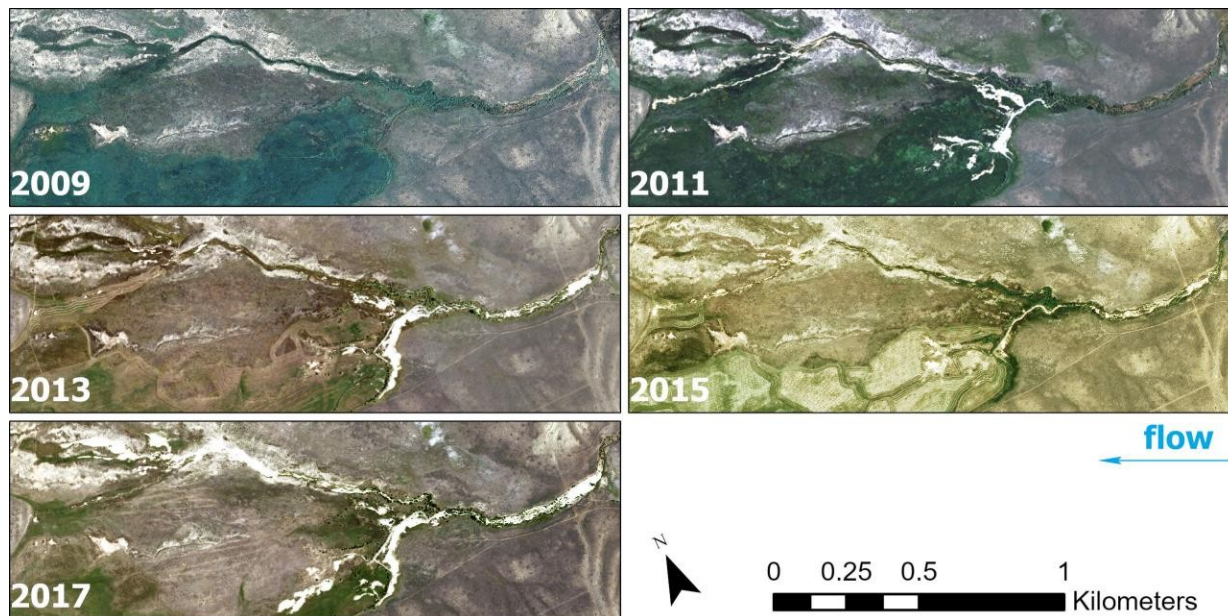


**Fig. 23.** NAIP imagery of the irrigation network diverted from North Sand Creek on State Line Ranch from 2009-2017 (USDA, 2009-2017). Channel widening and aggradation is evident beginning in 2011 and expands into other parts of the channel through 2017. The irrigation network was dredged between the 2013 and 2015 images, but the dredged area appears to have filled again with sand by 2017.

The results of this study also raise the question of whether the anthropogenically induced erosion of North Sand Hills is responsible for inducing the sediment wave. It is impossible to separate the effects of higher sediment influx and lower discharge when comparing the two creeks, and there are no historical geomorphological data on North Sand Creek with which to compare modern observations. However, given the State Line Ranch’s anecdotal observations of an unprecedented influx of sand to the irrigation network starting in 2011, the confirmation of this observation through remote sensing (Fig. 23), and finally the acknowledgement of the Colorado State Water Quality Control Commission (COWQCC, 2016), it does seem likely that

anthropogenic forces have at least exacerbated the North Sand Creek sediment wave, if not induced it entirely.

The BLM's strategy for reducing impact to North Sand Creek in the past has been to fence off certain areas of North Sand Hills to OHVs. During the summer of 2019, managers additionally fenced off most of the tributary to prevent users from riding directly in the channel. This research has shown that fenced-off areas have gained vegetation since 1984, while the unfenced areas have lost vegetation, indicating that the strategy does work to some degree. However, fenced-off areas on North Sand Hills have gained vegetative cover at a significantly slower rate than at East Sand Hills, which suggests they may be subject to continuing impact from elevated eolian transport on adjacent unfenced areas.

The negative impact to vegetation on North Sand Hills, especially in the vegetated areas that are not fenced-off to OHV users, is made all the more glaring by the Wilderness Study Area designation of most of the dunefield. These results indicate that the impacts of the North Sand Creek sediment wave might be mitigated by introducing more large wood to the channel; however, the downstream reaches of North Sand Creek are likely to continue to aggrade without substantial reduction of OHV visitor use hours on the dunefield and targeted restoration of dunefield vegetation.

#### *4.5 Conclusions and suggestions for future study*

These results yield three important conclusions about sediment waves: they can operate on annual scales in mixed eolian-fluvial environments, large wood can promote their dispersal, and the factors that determine their presence or absence may be subtle. North Sand Creek and East Sand Creek are similar in many ways and are subject to the same seasonal cycles of discharge and eolian influx. However, North Sand Creek's lower discharge and higher eolian influx appear to

exacerbate these effects to the point of initiating a sediment wave where it otherwise might not exist.

In this study, I documented conclusive incision throughout the study area, but did not document the aggradation which was likely taking place simultaneously downstream ~5.5 km, outside of my study area. Further research on North Sand Creek and East Sand Creek should extend the study area to the downstream reaches, including within the irrigation network of State Line Ranch. Measurement of sand depth was very straightforward within our study area because it was rarely more than a meter to the underlying coarser bed substrate. The reaches farther downstream, on the other hand, are underlain by deep alluvial and eolian deposits and this method would not be possible. Repeat measurement of established points or cross-sections with high-accuracy survey equipment or RTK GPS might be able to capture aggradation.

The timing and magnitude of the annual sediment wave at North Sand Creek is likely influenced by a variety of annual to decadal scale climatic factors, including: size and duration of the winter snowpack, wind speeds, flashy summer rainfall events, and El Niño / La Niña cycles. More sand is likely stored in the channel during low-flow years than high-flow years. Performing similar analyses in North Sand Creek and East Sand Creek in future years could yield better understanding of how these climatic factors influence sediment wave dynamics.

The results of this study suggest that annual sediment waves may take place in other mixed eolian-fluvial environments. Similar methods could be applied to other eolian-fluvial systems to determine what factors control the presence or absence of a sediment wave. Further study might reveal other locations where human impact in the watershed, including OHV recreation, might have contributed to sediment wave initiation. Eolian environments tend to be arid or semi-arid,

which on the one hand reduces the likelihood of impact to water resources, but on the other hand amplifies impact when it does occur.

## References

- Abatzoglou, J.T. & Williams, A.P. (2016). Impact of anthropogenic climate change on wildfire across western US forests. *Proceedings of the National Academy of Sciences* 113(42): 11770-11775. doi:10.1073/pnas.1607171113
- Ahlbrandt, T.S. & Andrews, S. (1978). Distinctive sedimentary features of cold-climate eolian deposits, North Park, Colorado. *Paleogeography, Paleoclimatology, Palaeoecology* 25: 327-351. doi:10.1016/0031-0182(78)90048-2
- Anderson, R.S. & Anderson, S.P (2010). *Geomorphology: the mechanics and chemistry of landscapes*. Cambridge University Press.
- Belward, A.S. & Skøien, J.O. (2015). Who launched what, when and why; trends in global land-cover observation capacity from civilian earth observation satellites. *ISPRS Journal of Photogrammetry and Remote Sensing* 103: 115-128. <https://doi.org/10.1016/j.isprsjprs.2014.03.009>
- Boyer, J.M. (2015). Written testimony of Dr. Jean Marie Boyer, PE, Hydros Consulting Inc. in support of the proposal to list a portion of segment COUCNP04a (Sand Creek) as impaired for sediment.
- Brummer, C.J. & Montgomery, D.R. (2006). Influence of coarse lag formation on the mechanics of sediment pulse dispersion in a mountain stream, Squire Creek, North Cascades, Washington, United States. *Water Resources Research* 42. doi:10.1029/2005WR004776 <https://doi.org/10.1029/2005WR004776>
- Bureau of Land Management (BLM) (2012). *6330- Management of Wilderness Study Areas (Public)*.
- Bureau of Land Management (BLM) (2018). *Public Land Statistics 2017*.
- Bureau of Land Management (BLM) (2018). *North Sand Hills OHV Area*. Retrieved from <https://www.blm.gov/visit/search-details/16697/2>
- Bureau of Land Management (BLM) (2020). *Killpecker Sand Dunes Open Play Area Campground*. Retrieved from <https://www.blm.gov/visit/killpecker-sand-dunes-open-play-area-campground>
- Colorado Climate Center (COCC) (2020). Walden weather station data. Retrieved from [https://climate.colostate.edu/data\\_access.html](https://climate.colostate.edu/data_access.html)
- Colorado Water Quality Control Commission (COWQCC) (2016). *Regulation #93: Colorado's Section 303(D) List of Impaired Waters*.
- Cortés, G, Giroto, M. & Margulis, S.A. (2014). Analysis of sub-pixel snow and ice extent



- over the extratropical Andes using spectral unmixing of historical Landsat imagery. *Remote Sensing of the Environment* 141: 64-78. doi:10.1016/j.rse.2013.10.023
- Cui, Y., Parker, G., Lisle, T.E., Gott, J., Hansler-Ball, M.E., Puzzuto, J.E., Allmendinger, N.E. & Reed, J.M. (2003). Sediment pulses in mountain rivers: Experiments. *Water Resources Research* 39(9): 1239-1251. doi:10.1029/2002WR001803
- East, A.E., Pess, G.R., Bountry, J.A., Magirl, C.S., Ritchie, A.C., Logan, J.B...Shafroth, P.B. (2015). Large-scale dam removal on the Elwha River, Washington, USA: River channel and floodplain geomorphic change. *Geomorphology* 228: 765-786. doi:10.1016/j.geomorph.2014.08.028
- Ferrer-Boix, C., Martín-Vide, J.P. & Parker, G. (2014). Channel evolution after dam removal in a poorly sorted sediment mixture: Experiments and numerical model. *Water Resources Research* 50: 8997-9019. doi:10.1002/2014WR015550
- Gilbert, G.K. (1917). Hydraulic-mining debris in the Sierra Nevada. *USGS Professional Paper* 105.
- Gran, K.B & Czuba, J.A. (2017). Sediment pulse evolution and the role of network structure. *Geomorphology* 277: 17-30. doi:10.1016/j.geomorph.2015.12.015
- Hoffman, D.F. & Gabet, E. J. Effects of sediment pulses on channel morphology in a gravel-bed river. *GSA Bulletin* 119(1/2): 116-125. doi:10.1130/B25982
- Iverson, R.M., Hinckley, B.S. & Hallett, B. (1981). Physical Effects of Vehicular Disturbances on Arid Landscapes. *Science* 212: 915-916. doi:10.1126/science.212.4497.915
- Keshava, N. (2003). A Survey of Spectral Unmixing Algorithms. *Lincoln Laboratory Journal* 14(1): 55-78.
- Knighton, A.D. (1989). River adjustment to changes in sediment load: the effects of tin mining on the Ringarooma River, Tasmania, 1875-1984. *Earth Surface Processes and Landforms* 14: 333-359. doi:10.1002/esp.3290140408
- Lenth, R. (2009). emmeans: Estimated Marginal Means, aka Least-Squares Means. R package version 1.4.2. <https://CRAN.R-project.org/package=emmeans>
- Lisle, T.E. Pizzuto, J.E. Ikeda, H., Iseya, F. & Kodama, Y. (1997). Evolution of a sediment wave in an experimental channel. *Water Resources Research* 33(8): 1971-1981. doi:10.1029/97WR01180
- Luckenbach, R.A. & Bury, R.B. (1983). Effects of off-road vehicles on the biota of the Algodones dunes, Imperial County, California. *Journal of Applied Ecology* 20: 265-286. doi:10.2307/2403392

- Lymburner, L., Bunting, P., Lucas, R., Scarth, P., Alam, I., Phillips, C., Ticehurst, C. & Held, A. (2020). Mapping the multi-decadal mangrove dynamics of the Australian coastline. *Remote Sensing of the Environment* 238: 111-185. doi:10.1016/j.rse.2019.05.004
- Madej, M.A. & Ozaki, V. (1995). Channel response to sediment wave propagation and movement, Redwood Creek, California, USA. *Earth Surface Processes and Landforms* 21: 911-927. doi:10.1002/(SICI)1096-9837(199610)21:10<911::AID-ESP621>3.0.CO;2-1
- Marion, D.A., Phillips, J.D., Yocum, C. & Mehlhope, S.H. (2014). Stream channel responses and soil loss at off-highway vehicle stream crossings in the Ouachita National Forest. *Geomorphology* 216: 40-52. doi:10.1016/j.geomorph.2014.03.034
- Meade, R.H. (1985). Wavelike Movement of Bedload Sediment, East Fork River, Wyoming. *Environmental Geology and Water Sciences* 7(4): 215-225. doi:10.1007/BF02509922
- Miller, D. J. & Benda, L.E. (2000). Effects of punctuated sediment supply on valley-floor landforms and sediment transport. *GSA Bulletin* 112(12): 1814-1824. doi:10.1130/0016-7606(2000)112<1814:EOPSSO>2.0.CO2
- Nakamura, F. (1966). Chronological Study on the Torrential Channel Bed by the Age Distribution of Deposits. *Research Bulletins of the College Experimental Forests* 43(1): 1-26.
- United States Department of Agriculture (USDA) (2009, 2011, 2013, 2015, 2017). National Aerial Imagery Program (NAIP). Obtained from USGS Earth Explorer [https://www.usgs.gov/centers/eros/science/usgs-eros-archive-aerial-photography-national-agriculture-imagery-program-naip?qt-science\\_center\\_objects=0#qt-science\\_center\\_objects](https://www.usgs.gov/centers/eros/science/usgs-eros-archive-aerial-photography-national-agriculture-imagery-program-naip?qt-science_center_objects=0#qt-science_center_objects)
- Nauman, T.W., Duniway, M.C., Webb, N.P. & Belnap, J. (2018). Elevated eolian sediment transport on the Colorado Plateau, USA: The role of grazing, vehicle disturbance, and increasing aridity. *Earth Surface Processes and Landforms* 43: 2897-2914. doi:10.1002/esp.4457
- Nelson, A. & Dubé, K. (2016). Channel response to an extreme flood and sediment pulse in a mixed bedrock and gravel-bed river. *Earth Surface Processes and Landforms* 41: 178-195. doi:10.1002/esp.3843
- Ouren, D.S., Haas, C., Melcher, C.P., Stewart, S.C., Ponds, P.D., Sexton, N.R., Burris, L., Fancher, & Bowen, Z.H. (2007). *Environmental effects of off-highway vehicles on Bureau of Land Management lands: A literature synthesis, annotated bibliographies, extensive bibliographies, and internet resources*. USGS Open-File Report.
- Pace, K.M., Tullos, D., Walter, C., Lancaster, S. & Segura, C. (2017). Sediment pulse behavior

- following dam removal in gravel-bed rivers. *River Research and Applications* 33:102-112. doi:10.1002/rra.3064
- Paige, A. D. & Hickin, E. D. (2000). Annual bed-elevation regime in the alluvial channel of Squamish River, southwestern British Columbia, Canada. *Earth Surface Processes and Landforms* 25: 991-1009.  
doi:10.1002/1096-9837(200008)25:9<991::AID-ESP113>3.0.CO;2-W
- Pickup, G., Higgins, R.J. & Grant, WE. (1983). Modeling sediment transport as a moving wave—the transfer and deposition of mining waste. *Journal of Hydrology* 60: 281-301.  
doi:10.1016/0022-1694(83)90027-6
- Pierson, T.C., Pringle, P.T. & Cameron, K.A. (2011). Magnitude and timing of downstream channel aggradation and degradation in response to a dome-building eruption at Mount Hood, Oregon. *GSA Bulletin* 123(1/2): 3-20. doi:10.1130/B30127.1
- Pryor, B.S., Lisle, T., Montoya, D.S. & Hilton, S. (2011). Transport and storage of bed material in a gravel-bed channel during episodes of aggradation and degradation: a field and flume study. *Earth Surface Processes and Landforms* 36: 2028-2041. doi:10.1002/esp.2224
- Roberts, R.G. & Church, M. (1986). The sediment budget in severely disturbed watersheds, Queen Charlotte Ranges, British Columbia. *Canadian Journal of Forest Research* 16(5): 1092-1106. doi:10.1139/x86-189.
- Short Elliott Hendrickson, Inc. (SEH) (2007). *Jackson County, Colorado: North Sand Hills Master Plan*.
- Short, L.E., Gabet, E.J. & Hoffman, D.F. (2015). The role of large woody debris in modulating the dispersal of a post-fire sediment pulse. *Geomorphology* 246: 351-358.  
doi:10.1016/j.geomorph.2015.06.031
- Sun, D. (2015). Detection of dryland degradation using Landsat spectral unmixing remote sensing with syndrome concept in Minqin County, China. *International Journal of Applied Earth Observation and Geoinformation*. 41: 34-45.  
doi:10.1016/j.jag.2015.04.015
- Sutherland, D.G., Ball, M.H., Hilton, S.J. & Lisle, T.E. (2002). Evolution of a landslide-induced sediment wave in the Navarro River, California. *Geological Society of America Bulletin* 114(8): 1036-1048. doi:10.1130/0016-7606(2002)114<1036:EOALIS>2.0.CO;2
- Tuttle, M. & Griggs, G. (1987). Soil Erosion and Management Recommendations at Three State Vehicular Recreation Areas, California. *Environmental Geology and Water Sciences* 10(2): 111-123. doi:10.1007/BF02574669
- Ta, W., Wang, H. & Jia, X. (2015). The contribution of eolian processes to fluvial sediment yield

from a desert watershed in the Ordos Plateau, China. *Hydrological Processes* 29: 80-89. doi:10.1002/hyp.10137

United States Geological Survey (USGS) (1989). National Aerial Photography Program (NAPP). Obtained from USGS Earth Explorer  
[https://www.usgs.gov/centers/eros/science/usgs-eros-archive-aerial-photography-national-aerial-photography-program-napp?qt-science\\_center\\_objects=0#qt-science\\_center\\_objects](https://www.usgs.gov/centers/eros/science/usgs-eros-archive-aerial-photography-national-aerial-photography-program-napp?qt-science_center_objects=0#qt-science_center_objects)

United States Geological Survey (USGS) (2016). The StreamStats program for Colorado. Retrieved from <https://streamstats.usgs.gov/ss/>

United States Geological Survey (USGS) (2020a). USGS Landsat 5 Surface Reflectance Tier 1. Obtained from Google Earth Engine  
[https://developers.google.com/earth-engine/datasets/catalog/LANDSAT\\_LT05\\_C01\\_T1\\_SR](https://developers.google.com/earth-engine/datasets/catalog/LANDSAT_LT05_C01_T1_SR)

United States Geological Survey (USGS) (2020b). USGS Landsat 8 Surface Reflectance Tier 1. Obtained from Google Earth Engine  
[https://developers.google.com/earth-engine/datasets/catalog/LANDSAT\\_LC08\\_C01\\_T1\\_SR](https://developers.google.com/earth-engine/datasets/catalog/LANDSAT_LC08_C01_T1_SR)

United States Geological Survey (USGS) (2020c). National Water Information System data for gage 006620000 North Platte River near Northgate, CO.

Vose, J.M., Clark, J.S., Luce, C.H., Patel-Weynand, T., 2016. Effects of Drought on Forests and Rangelands in the United States: A Comprehensive Science Synthesis. United States Department of Agriculture General Technology Report WO-93b.

Western Regional Climate Center (WRCC) (2020). Walden, Colorado Period of Record Monthly Climate Summary. Retrieved from  
<https://wrcc.dri.edu/cgi-bin/cliMAIN.pl?cowald>

Wohl, E. & Scott, D.N. (2016). Wood and sediment storage and dynamics in river corridors. *Earth Surface Processes and Landforms* 42: 5-23. doi:10.1002/esp.3909

Xu, J., Yang, J. & Yan, Y. (2006). Erosion and sediment yields as influenced by coupled eolian and fluvial processes: The Yellow River, China. *Geomorphology* 73: 1-15. doi:10.1016/j.geomorph.2005.03.012

Yan, N. & Baas, A.C.W. (2018). Transformation of parabolic dunes into mobile barchans triggered by environmental change and anthropogenic disturbance. *Earth Surface Processes and Landforms* 43: 1001-1018. doi:10.1002/esp.4299

## Appendix A: Repeat Photography



NP8 (H): Oversteepened sand bank in June indicates recent incision. Consistent bed material of mixed cobbles, gravels, and sand throughout June and July, evident aggradation by aeolian sand in August through November.



NP7 (G): Oversteepened sand bank in July indicates recent incision. Consistent bed material of mixed cobbles, gravels, and sand throughout June and July, evident aggradation by aeolian sand in August through November.



NP6 (H): A wide, sand-bedded channel in May and early June, narrowing and incising by about 2 vertical meters in mid-June, exposing scattered cobbles in the bed. Incision is evidently accompanied by gravitational slumping of the right bank. The channel does not notably change through November.



**NP5 (H/G):** During June and July the channel narrows and incises, then remains in a similar morphology through November. The reach remains sand-bedded throughout the study period.

**NP3 (G):** Rapid incision is evident between 5/16 and 5/18, following stability since November of the previous year. <1 m-tall SASS form during June and July as the channel incises and migrates. The dune slope relaxes, possibly due to aeolian transport, and the channel aggrades between August and November. The reach remains sand-bedded throughout the study period.



NP2 (G): Watershed snowmelt is already mostly complete by 5/15, though there is no visible sand in the channel bed at the confluence with the dune front-tributary and the mainstem. A high concentration of sand bedload appears suddenly on 5/19, and it remains similarly high until August when flow becomes low. There are no indicators of aggradation or incision evident throughout the study period.

NP1 (H): Over the course of the summer, the channel narrows and becomes visually less turbid. By mid-July scattered cobbles are visible in the bed, which indicates incision, though it is not as dramatic as the repeat photo locations of the upstream zone.



**EP7 (H):** No indicators for either incision or aggradation evident throughout the study period. The bed material remains a mix of cobbles and sand.



**EP6 (G):** A <1 m tall SAS on first observation in June indicates recent aggradation followed by incision. The SAS is destroyed in June. The channel bed material remains a mix of sand and gravel throughout the study period.



**EP5 (G):** No indicators for either incision or aggradation evident throughout the study period. The reach remains sand-bedded throughout the study period.





EP4 (H): No indicators for either incision or aggradation. The bed material remains a mix of sand, gravel, and cobbles throughout the study period.



EP3 (H): No indicators for either incision or aggradation. The bed material remains a mix of sand and gravel throughout the study period.



EP2 (H): The reach is sand-bedded throughout June and July. Some gravel appears in August which was not visible before, potentially indicating incision.



EP1 (H): No indicators of either incision or aggradation. The reach remains sand-bedded throughout the study period.

## Appendix B: Logjam Sand Wedge Measurements

### Key

Week: Number of weeks since 5/16/2019

U Depth: Sand wedge depth upstream of logjam

D Depth: Sand wedge depth downstream of logjam

V: Estimated sand wedge volume

Week	LJ ID	U Depth (cm)	D Depth (cm)	UL (m)	V (m <sup>3</sup> )
1	N1	40	10	13	12.6
1	N2	48	30	450	188.6
1	N3	64	39	60	222.1
1	N4	47	46	14.35	26.4
1	N5	77	12	21	74.7
1	N6	54	54	15.05	29.2
1	N7	56	35	170	358
1	N8	28	14	4.3	0.9
1	N9	34	5	3.9	2.3
1	N10	3	17	3.4	0.3
1	N11	44	20	5	0.6
1	N13	32	31	9.6	2.9
1	N14	55	24	1.6	0.7
1	N15	35	23	2.9	1.5
1	NJ16	124	32	620	2913.4
1	N17	58	3	50.5	60.9
1	N18	59	5	250	363.9
3	N1	41	23	13	24
3	N2	43	34	450	381.4
3	N3	69	32	60	146.3
3	N4	24	4	14.35	16.8
3	N5	44	12	21	30.7
3	N6	51	22	15.05	41.4
3	N7	42	25	170	360.5
3	N8	21	15	4.3	0.9
3	N9	21	9	3.9	1.5
3	N10	25	13	3.4	1.2
3	N11	46	25	5	2.3
3	N13	26	18	9.6	1.9
3	N14	47	4	1.6	1.4
3	N15	52	43	2.9	1.9
3	NJ16	124	30	620	3897.2
3	N17	54	40	50.5	93.7
3	N17.5	32	33	8.6	5.7

3	N18	29	22	39	43.2
3	N19	48	19	8	4.6
5	N1	49	7	13	29.9
5	N2	22	24	450	235.1
5	N3	37	10	17.2	19.3
5	N4	41	0	7.5	11.3
5	N5	32	0	21	20.9
5	N6	52	7	15.05	69.6
5	N7	7	46	0	0
5	N8	18	10	4.3	1.1
5	N9	19	12	3.9	1.2
5	N10	29	25	3.4	1.3
5	N11	56	28	5	4.8
5	N11.5	43	40	7	4.1
5	N13	29	19	9.6	2
5	N14	64	14	1.6	1.5
5	N15	28	20	2.9	1.2
5	NJ16	124	21	330	1432.2
5	N17	66	46	50.5	66
5	N17.5	40	40	7	4.9
5	N18	41	29	51.7	47.3
5	N19	51	12	8.3	8.8
7	N1	52	16	13	40.3
7	N2	41	47	189	119.1
7	N3	30	17	28.2	25.4
7	N4	48	4	14.35	26.7
7	N5	31	14	21	24
7	N6	65	15	10.7	29.9
7	N7	22	46	8.6	3.8
7	N8	26	8	4.3	1.7
7	N9	17	23	3.9	1.6
7	N10	23	20	3.4	1.6
7	N11	39	31	5	5.6
7	N11.5	74	32	130	183.6
7	N13	59	2	9.6	5.9
7	N14	59	2	1.6	1.4
7	N15	28	26	2.9	1.9
7	NJ16	124	15	330	1432.2
7	N17	67	46	14.7	17.7
7	N17.5	23	3	7.9	4.3
7	N18	36	28	0.36	0.4
7	N19	35	5	7.4	5.8
9	N1	46	21	13	34.1

9	N2	31	57	97.6	39.3
9	N3	30	11	18	4.9
9	N4	27	12	7.5	6.5
9	N5	43	2	13.5	13.8
9	N6	38	5	14.6	22.2
9	N7	26	27	2.4	0.4
9	N9	26	11	1.9	0.2
9	N11	17	17	3.8	0.4
9	N11.5	24	18	2.9	0.4
9	N13	28	28	0	0
9	N14	46	6	1.5	0
9	N15	32	30	2.9	0
9	NJ16	124	35	330	0
9	N17	35	54	47.9	8.5
9	N17.5	63	15	6.3	2.6
9	N18	22	34	62.4	8.8
9	N19	35	10	7.7	4.2
12	N1	18	38	15.3	21.4
12	N2	18	60	5	1.1
12	N3	21	26	9.3	1.8
12	N4	41	39	5.6	3.4
12	N5	23	18	12	6.1
12	N6	43	20	14.3	13.6
12	N7	14	48	3.2	0.2
12	N9	19	26	1.7	0.2
12	N11	10	22	5.1	0.7
12	N11.5	38	16	1.6	0.4
12	N17	92	66	46.5	0
12	N17.5	21	12	22	0
12	N18	29	35	52.9	0
12	N19	35	8	7	0
14	N1	56	10	9.8	5.2
14	N2	7	39	0	0
14	N3	0	28	0	0
14	N4	30	22	6.7	2
14	N5	18	20	9.8	2.2
14	N6	24	3	17	12.1
14	N7	22	47	1.6	0.8
14	N9	18	21	1.5	0.1
14	N11	12	18	2.3	0.1
14	N11.5	20	4	2.3	0.2
3	E1	72	18	4.7	6.8
3	E2	77	7	30.7	47.3

3	E3	34	0	10.4	8.2
3	E4	14	11	0	0
3	E5	20	0	10	4
3	E6	5	7	0	0
3	E7	36	35	7.4	11.7
3	E8	33	0	6	4.5
3	E9	110	10	63	311.9
3	E10	88	0	20	56.5
3	E11	103	15	0.3	1.4
3	E12	79	0	49	71.3
3	E13	81	0	18.4	30.7
3	E14	16	0	0	0.2
3	E16	51	21	4.8	5.6
3	E17	57	0	10	12.2
3	E18	32	11	8.5	6.7
3	E19	14	0	0	0.9
3	E20	17	0	0	1
3	E21	11	0	0	1
3	E22	16	0	0	1.9
3	E24	15	0	0	2.7
3	E25	42	0	0	3
3	E26	20	0	0	1.3
5	E1	82	0	4.7	9.6
5	E2	51	6	26.7	35.6
5	E3	71	0	15	29.2
5	E4	17	25	3.4	1
5	E5	42	3	4	2.8
5	E6	0	17	0	0
5	E7	42	18	1.2	1.3
5	E7.5	38	26	12.9	9.8
5	E8	31	8	4.6	3.4
5	E9	67	0	45	131.8
5	E10	41	0	0	2.3
5	E11	63	16	8.8	11.6
5	E12	64	11	30.9	51.4
5	E13	89	7	12	21.8
5	E14	11	0	0	0.4
5	E15.5	23	0	16.6	10.7
5	E16	27	5	4.7	2.9
5	E17	29	13	8.2	6.5
5	E18	5	0	0	0.2
5	E19	3	0	0	0
5	E20	5	0	0	0.4

5	E21	7	0	0	0.2
5	E22	10	0	0	0.6
5	E24	12	0	0	2.2
5	E25	10	0	0	0.6
5	E26	8	0	0	0.4
7	E1	32	0	6.6	3.7
7	E2	71	2	24.3	48.1
7	E3	44	0	28.3	34.9
7	E4	22	12	27	8.8
7	E5	29	1	10.2	6.1
7	E6	0	8	0	0
7	E7	17	25	10	4.6
7	E7.5	60	10	10.3	13.3
7	E8	37	3	0	7
7	E9	73	6	39.2	98.7
7	E10	11	0	0	0.8
7	E11	56	11	10	14.9
7	E12	53	9	8.4	8.7
7	E13	48	7	2.9	2.1
7	E14	0	7	0	0
7	E15.5	20	0	11	3.3
7	E16	50	9	3.8	3.3
7	E17	27	3	3.7	2.2
7	E18	29	6	0	1.4
7	E19	3	0	0	0
7	E20	0	0	0	0
7	E21	3	0	0	0
7	E22	9	0	0	0.4
7	E24	4	0	0	0.5
7	E25	45	0	0	2.8
7	E26	10	0	0	0.2
9	E1	27	27	25	10
9	E2	14	10	3.7	0.7
9	E3	26	8	15.7	9.7
9	E4	32	10	19.7	11.7
9	E5	27	0	9.7	4.6
9	E6	0	8	0	0
9	E7	10	41	9.4	2.5
9	E7.5	69	29	9.3	9.3
9	E8	20	14	4.4	1.9
9	E9	69	0	33.4	95.6
9	E10	43	0	10	6.5
9	E11	73	19	41.3	69.7

9	E12	43	0	0	3.9
9	E13	55	2	10.5	7.3
9	E14	33	0	18.6	8.7
9	E15.5	8	1	0	0.2
9	E16	7	3	0	0
9	E17	25	0	50	51
9	E18	15	20	0	1.4
9	E19	9	3	0	0
9	E20	5	10	0	0
9	E21	6	2	0	0
9	E22	7	6	0	0.3
9	E24	5	0	0	0
9	E25	9	0	0	0
9	E26	6	0	0	0
12	E1	49	41	22.7	16.6
12	E2	12	6	4.9	0.7
12	E3	45	5	24.4	21.3
12	E4	32	16	28	15.8
12	E5	26	8	9.8	4.4
12	E6	5	9	0	0
12	E7	4	45	18.9	0.6
12	E7.5	52	31	4.7	3.7
12	E8	18	12	13.1	3.2
12	E9	78	6	39.6	49.6
12	E10	48	0	11.7	4.2
12	E11	66	24	40.1	50
12	E12	31	9	0	1.5
12	E13	36	2	6.7	3.2
12	E14	32	0	23.7	8.3
12	E15.5	5	0	0.03	0
12	E16	0	4	0	0
12	E17	30	0	50	30
12	E18	22	22	8.6	3.8
12	E19	33	11	3.1	1.3
12	E20	12	59	7.2	1.6
12	E21	12	7	0	0
12	E22	18	27	19.8	6.8
12	E24	26	9	3.9	1.2
12	E25	18	2	7	1.2
12	E26	21	36	0	0.3
14	E1	31	32	21.3	8
14	E2	42	0	0	8.2
14	E3	42	13	12.2	3.3



14	E4	36	21	25.2	12.2
14	E5	27	17	7.2	2.1
14	E6	2	21	0	0
14	E7	29	110	13.8	3.6
14	E7.5	33	15	4	1.6
14	E8	23	18	4.2	0.7
14	E9	72	4	56.6	117.6
14	E10	48	5	10.5	6
14	E11	55	27	38.1	43.2
14	E12	27	2	3.2	0.6
14	E13	34	19	12.3	8.6
14	E14	38	11	9.9	3.8
14	E15.5	0	0	0	0
14	E16	0	2	0	0
14	E17	41	29	50	65.1
14	E18	41	43	7.7	2.8
14	E19	25	17	2.7	0.4
14	E20	7	55	2.5	0.3
14	E21	9	7	1.5	0.1
14	E22	20	21	12.6	2.4
14	E24	20	28	4.8	0.8
14	E25	4	0	0	0
14	E26	7	35	0	0